Astronomy & Astrophysics manuscript no.
(will be inserted by hand later)

arXiv:astro-ph/0305472 v1 23 May 2003

An Hα survey aiming at the detection of extraplanar diffuse ionized gas in halos of edge–on spiral galaxies ⋆

II. The Hα survey atlas and catalog

J. Rossa ⋆⋆[1,2] and R.–J. Dettmar[1]

[1] Astronomisches Institut, Ruhr–Universität Bochum, D–44780 Bochum, Germany
e-mail: jrossa@stsci.edu, dettmar@astro.ruhr-uni-bochum.de
[2] Space Telescope Science Institute, 3700 San Martin Drive, Baltimore, MD 21218, U.S.A. (present address)

Received 14 February 2003 / Accepted 6 May 2003

Abstract. In this second paper on the investigation of extraplanar diffuse ionized gas in nearby edge–on spiral galaxies we present the actual results of the individual galaxies of our Hα imaging survey. A grand total of 74 galaxies have been studied, including the 9 galaxies of a recently studied sub–sample (Rossa & Dettmar 2000). 40.5% of all studied galaxies reveal extraplanar diffuse ionized gas, whereas in 59.5% of the survey galaxies no extraplanar diffuse ionized gas could be detected. The average distances of this extended emission above the galactic midplane range from 1–2 kpc, while individual filaments in a few galaxies reach distances of up to $|z| \sim 6$ kpc. In several cases a pervasive layer of ionized gas was detected, similar to the Reynolds layer in our Milky Way, while other galaxies reveal only extended emission locally. The morphology of the diffuse ionized gas is discussed for each galaxy and is compared with observations of other important ISM constituents in the context of the disk–halo connection, in those cases where published results were available. Furthermore, we present the distribution of extraplanar dust in these galaxies, based on an analysis of the unsharp–masked R–band images. The results are compared with the distribution of the diffuse ionized gas.

Key words. galaxies: halos – galaxies: spiral – galaxies: starburst – galaxies: ISM – galaxies: structure

1. Introduction

Our current knowledge of the morphology of the extraplanar diffuse ionized gas (eDIG) in normal (non–starburst) edge–on spiral galaxies rests on a few investigations of small galaxy samples (Pildis et al. 1994; Rand 1996; Hoopes et al. 1999; Rossa & Dettmar 2000), as well as on some additional studies of individual galaxies (e.g., Dettmar 1990; Rand et al. 1992; Ferguson et al. 1996; Domgörgen & Dettmar 1997). There have been a few galaxies studied during the last decade, however, the question was raised, whether or not the presence of eDIG is a common phenomenon among all types of galaxies, or whether it is indeed a direct consequence of the strength of the star formation activity, both on local and global scales (Rand 1996; Rossa & Dettmar 2000). To answer this question a systematic investigation is obligatory. We have therefore conducted, for the first time, a large survey of nearby *non–starburst* edge–on spiral galaxies, aiming at a quantitative morphological study of gaseous halos, based on the broad coverage of the strength of SF activity in the underlying galaxy disks (i.e. broad coverage of $L_{\rm FIR}$) of these galaxies. We present the observed morphological results, based on the Hα imaging observations, and describe the derived DIG characteristics for each galaxy in this paper in greater detail. For information on the scientific background on eDIG and its detection in external galaxies we refer the reader to our previous works (Rossa & Dettmar 2000, 2003), and references therein and to some older review articles (Dettmar 1992; Dahlem 1997) for a more detailed overview on this topic.

The current paper is structured as follows. In Sect. 2 we present some details on the observations and data reduction procedures. In Sect. 3 we show the actual results for the galaxies, while in Sect. 4 we discuss the extraplanar dust. Then the atlas is presented (available only electron-

Send offprint requests to: J. Rossa

⋆ Based on observations collected at the European Southern Observatory, Chile (ESO No. 63.N–0070, ESO No. 64.N–0034, ESO No. 65.N.–0002). Figures 22-54 are only available in electronic form at http://www.edpsciences.org

⋆⋆ Visiting Astronomer, German–Spanish Astronomical Centre, Calar Alto, operated by the Max–Planck–Institute for Astronomy, Heidelberg, jointly with the Spanish National Commission for Astronomy.

ically at EDP Sciences), where we display two galaxies on each page. Each of the two columns per page consists of the R–band (top), the unsharp–masked R–band (middle), and the continuum subtracted Hα image (bottom). Finally, in Sect. 5 we summarize briefly the results.

2. Observations and data reduction

2.1. Hα observations

The edge–on spiral galaxies, which form the basis of this Hα survey, have been observed in five individual observing runs between 1999 and 2000. The northern hemisphere objects (Runs NH–1, NH–2) have been observed with the CAHA[1] 2.2 m telescope at the Calar Alto Observatory in southern Spain, and the southern hemisphere objects (Runs SH–1, SH–2, SH–3) have been observed with the Danish 1.54 m telescope at the European Southern Observatory at La Silla/Chile (see Table 1 for a summary of the individual observing runs). Six additional targets, that were selected on the basis of our selection criteria, have also been included into this survey. These were galaxies, already observed several years ago in past observing runs, or that were at our disposal, so we did not have to re–observe them (Runs SH–a, SH–b, SH–c). The basic galaxy properties, including the coordinates, galaxy types, distances, radial velocities, sizes, inclinations, and magnitudes, are listed in Table 2.

Table 1. Individual observing runs for the new Hα survey

Run No.	Dates	Telescope
NH–1	19–22/02/1999	CAHA2.2
NH–2	08–13/08/1999	CAHA2.2
SH–1	07–10/07/1999	DAN1.54
SH–2	09–13/11/1999	DAN1.54
SH–3	29/07–01/08/2000	DAN1.54
SH–a	22/02/1993	ESO2.2
SH–b	07–08/05/1991	NTT
SH–c	10/02/1995	NTT

The observations for the northern hemisphere galaxies have been performed with CAFOS[2] in direct imaging mode, attached to the CAHA 2.2 m telescope. The used CCD chip was a 2048 × 2048 pixel SITe#1d, with a pixel size of 24μm. The pixel scale was $0\farcs53\,\mathrm{pix}^{-1}$, and the resulting field of view was $18\farcm1 \times 18\farcm1$. The used Hα filters were the CA #658/10 and the CA #665/17 filters with a $\Delta\lambda = 98$ Å and 168 Å, respectively. The used R–band filter (Johnson R) was the CA #641/158 with $\Delta\lambda = 1575$ Å.

The southern hemisphere galaxies have been observed with DFOSC[3] in imaging mode, attached to the Danish 1.54 m telescope at La Silla/Chile. The used CCD camera

[1] Centro Astronómico Hispano Alemán
[2] Calar Alto Faint Object Spectrograph
[3] Danish Faint Object Spectrograph Camera

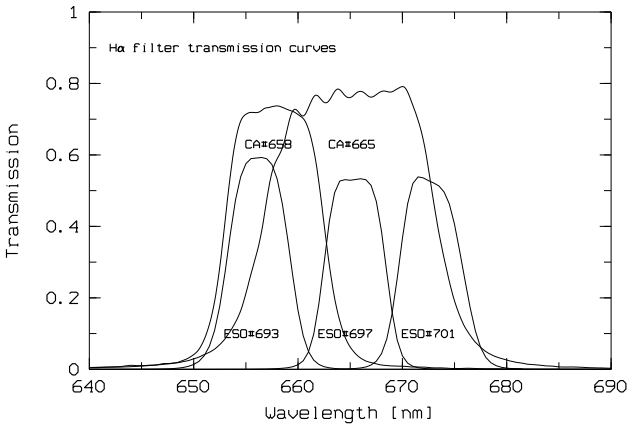

Fig. 1. Transmission curves for the ESO and Calar Alto Hα filters (ESO #693, #697, #701 and CA #658/10, CA #665/17), respectively. The plot has been generated in the MIDAS environment with the use of the implemented ESO filter and edited CAHA filter table–files.

was a LORAL/LESSER 2 k × 2 k chip with a pixel size of 15μm. The pixel scale was $0\farcs39\,\mathrm{pix}^{-1}$, and the maximum field of view (fov) was $13\farcm7 \times 13\farcm7$. Due to vignetting effects at the borders of the filters we have used only the inner 1601 × 1601 pixels of the CCD chip in most cases, yielding a fov of $10\farcm4 \times 10\farcm4$. The used Hα filters were the ESO #693, #697, and #701 filters with a $\Delta\lambda = 62.1$ Å, 61.6 Å, and 63.1 Å, respectively. The broad–band observations, to be used for the continuum subtraction, have been acquired through the ESO #452 (Bessel R) filter, which has a $\Delta\lambda = 1647$ Å. Instrumental parameters for six additional objects can be found elsewhere (Rossa & Dettmar 2000). The Hα transmission curves of the filters, which have been used for this survey, are shown in Fig. 1. A journal of observations for our galaxies is given in Table 3.

2.2. Data reduction and analysis

The data reduction has been performed in the usual manner including bias level correction, flat–fielding, background correction, registering of the stars (alignment of the R–band image with respect to the Hα image), scaling of the R–band image, and final continuum subtraction. In almost all cases the Hα images (split into two individual exposures for cosmic ray removal) have been combined. All these reduction steps have been performed using various IRAF packages.

For the northern survey the bias correction was performed by using the IRAF *colbias* task, taking the information of the overscan region into account. This was appropriate, since the bias exposures showed diagonal stripes. For the southern hemisphere objects the bias correction was done using a *masterbias* frame (one per night) obtained from median combining individual bias frames of each night. The flat–field correction was done using a normalized flat–field image created from combining the

individual flat–field exposures for each filter separately. Final background correction was done by subtracting the mean sky countrates from the flat–field corrected object frames. These values were estimated from at least three regions on each object frame that were neither contaminated by cosmic–ray hits nor populated by stars. The R–band frames were aligned and shifted with respect to the Hα exposures before combining each of the two object exposures. Finally the R–band image was scaled to the Hα image. The scaling factor has been determined from the ratio of the countrates of individual foreground stars in the R–band and Hα images. Then the scaled R–band image was subtracted from the Hα image. Due to the given bandwidth of the used Hα filters also the adjacent [N II] emission is covered. For the sake of brevity we therefore always refer to the emission of Hα+[N II] when we speak of an Hα image. More details on the continuum subtraction are given in Sect. 3.3.

3. Results

3.1. General results

This current Hα survey comprises of 65 nearby edge–on galaxies. 59 of these galaxies have been observed during the course of this survey, whereas we have added 6 additional target galaxies, from which we had Hα data at our disposal. Taking the 9 edge–on galaxies from our first sample (Rossa & Dettmar 2000) into consideration, the survey covers 74 galaxies in total. From these 74 galaxies 63 actually are new observations, whereas 11 galaxies have already been investigated in the DIG context by other researchers. We have included them because we wanted some galaxies for an intercomparison between our sample and the samples studied by other investigators. Furthermore, we wanted to have a more homogeneous sample in the sense of FIR luminosity, and thus included also a very few starburst galaxies. Needless to say that many starbursts fulfilled our selection criteria, but we did not want to re–observe all targets, and were also primarily interested in the galaxies with lower SF activity. The description of the selection criteria for the Hα survey target galaxies are presented in detail in Paper I (Rossa & Dettmar 2003). Far below (Table 5) we present the DIG morphology of the sample galaxies with information on the vertical extent ($|z|$), and the radial extent of the star formation activity (R_{SF} [kpc]).

As already mentioned our extended survey, which includes the 9 previously investigated galaxies presented in an earlier work (Rossa & Dettmar 2000), consists of a grand total of 74 galaxies. 30 galaxies, that is almost 41% of our survey, show extraplanar DIG features (either a pervasive layer, and/or filaments, or plumes, etc.). Excluding the 9 galaxies (first sub–sample), there are still 24 galaxies out of 65 with eDIG detections left, that is $\sim$ 37% of the survey. As we were primarily aiming to trace the fainter end of the SF activity, we were selecting galaxies with a broader range of L_{FIR}, compared to the galaxies, which were studied earlier by Lehnert & Heckman (1995), which were selected only on the basis of being infrared warm galaxies ($S_{60}/S_{100} \geq 0.4$). Therefore, it is not surprising that we did detect a good fraction of galaxies with no extraplanar emission.

3.2. Results and notes on selected galaxies

In this subsection a brief description of the observed eDIG morphology of selected galaxies is presented in addition to some background information, relevant in the DIG context for those targets. The galaxies are listed according to their increasing Right Ascension. The Hα images of all survey galaxies are shown together with the accompanying broad band images (R–band, and unsharp–masked R–band image) in Figs. 22–54 (available only in electronic form at EDP Sciences). However, some enlargements of selected galaxies with characteristic and spectacular eDIG morphology are included in logarithmic scale as separate figures in this section, in order to highlight some finer details of eDIG emission. A comparison with observations by other researchers from various wavelength regimes in the context of the disk–halo interaction is made, whenever such observations were available in the literature.

NGC 24

The Hα morphology of NGC 24 comprises of planar DIG which is visible between several bright H II regions in the disk. No extraplanar DIG is detected which is basically due to the fact that this galaxy is not perfectly edge–on. Guthrie (1992) lists an inclination of 78°. Although the L_{FIR}/D_{25}^2 ratio (for a definition of this expression please cf. Paper I) is quite low, the S_{60}/S_{100} ratio is moderate, and as the Hα distribution implies there is considerable star formation activity all over the disk. Additional evidence comes from a UV–study of nearby galaxies, where the morphology of the nuclear region in NGC 24 was studied (Maoz et al. 1996). They classify NGC 24 as a galaxy with star-forming morphology, and several knots or compact sources can be identified on the UV ($\sim$2300 Å) image, obtained with the Faint Object Camera (FOC) on–board HST. These regions are either compact star clusters or individual OB stars.

UGC 260

UGC 260 is shown with another smaller edge–on galaxy, CGCG 434–012, located 2′.4 west of UGC 260 (see Fig. 21), which has a similar redshift ($\Delta v = 47\,\mathrm{km\,s^{-1}}$). Reshetnikov & Combes (1996) included them in their list of tidally–triggered disk thickening galaxies. Indeed, the morphology in the continuum–subtracted Hα image looks quite distorted. The H II regions are not aligned and just below the disk in the very northern part seems to be a small additional galaxy possibly in the process of merging, or this represents debris tidal tails. Extraplanar DIG is detected, representing a faint layer, with a few individual emission patches. The NED lists another galaxy pair

Table 2. Basic galaxy parameters

Galaxy[a]	alt. name	R.A. (J2000)	Dec. (J2000)	Type	D [Mpc]	$v_{\rm H\,I}$ [km s^{-1}]	$a \times b$	i	$m_{\rm B}$[b]
NGC 24	ESO 472–16	$00^{\rm h}09^{\rm m}56.6^{\rm s}$	$-24°57'53''$	Sc	6.8	554	$5.8' \times 1.3'$	77°	12.07
NGC 100	FGC 0042	$00^{\rm h}24^{\rm m}02.6^{\rm s}$	$+16°29'09''$	Sc	11.2	842	$5.7' \times 0.6'$	84°	14.00
UGC 260	FGC 0046	$00^{\rm h}27^{\rm m}02.9^{\rm s}$	$+11°35'03''$	Sc	28.5	2135	$2.7' \times 0.4'$	81°	13.71
ESO 540–16	FGC 0082	$00^{\rm h}42^{\rm m}14.9^{\rm s}$	$-18°09'40''$	SBcd	20.7	1555	$2.7' \times 0.3'$	84°	14.32
MCG-2-3-16	FGC 0090	$00^{\rm h}47^{\rm m}46.7^{\rm s}$	$-09°53'54''$	SBc	17.9	1345	$3.0' \times 0.4'$	82°	- - - -
NGC 360	ESO 79–14	$01^{\rm h}02^{\rm m}51.2^{\rm s}$	$-65°36'34''$	Sc	30.7	2302	$3.5' \times 0.4'$	83°	13.40
NGC 669	UGC 01248	$01^{\rm h}47^{\rm m}16.1^{\rm s}$	$+35°33'48''$	Sab	62.4	4677	$3.1' \times 0.6'$	79°	12.97
UGC 1281	FGC 0195	$01^{\rm h}49^{\rm m}32.4^{\rm s}$	$+32°35'32''$	Sc	4.6	157	$4.5' \times 0.8'$	80°	12.87
NGC 891	UGC 01831	$02^{\rm h}22^{\rm m}33.1^{\rm s}$	$+42°20'48''$	Sb	9.5	528	$14.0' \times 3.0'$	88°	10.84
UGC 2082	FGC 0317	$02^{\rm h}36^{\rm m}16.3^{\rm s}$	$+25°25'29''$	Sc	9.4	707	$5.4' \times 0.8'$	81°	13.56
IC 1862	ESO 356–15	$02^{\rm h}51^{\rm m}57.6^{\rm s}$	$-33°20'31''$	Sbc	85.3	6400	$2.8' \times 0.3'$	84°	14.45
NGC 1247	FGC 0396	$03^{\rm h}12^{\rm m}13.0^{\rm s}$	$-10°28'58''$	Sab	52.6	3945	$3.4' \times 0.5'$	82°	13.47
ESO 117–19	PGC 14337	$04^{\rm h}02^{\rm m}32.5^{\rm s}$	$-62°18'53''$	SBbc	71.1	5335	$2.0' \times 0.3'$	81°	14.58
IC 2058	ESO 157–18	$04^{\rm h}17^{\rm m}54.5^{\rm s}$	$-55°55'57''$	Sc	18.2	1368	$3.1' \times 0.4'$	83°	13.87
ESO 362–11	PGC 017027	$05^{\rm h}16^{\rm m}39.0^{\rm s}$	$-37°06'00''$	Sbc	17.9	1346	$4.7' \times 0.8'$	80°	13.04
ESO 121–6	FGCE 0562	$06^{\rm h}07^{\rm m}29.2^{\rm s}$	$-61°48'25''$	Sc	16.2	1211	$3.9' \times 0.7'$	80°	13.43
NGC 2188	ESO 364–37	$06^{\rm h}10^{\rm m}09.5^{\rm s}$	$-34°06'22''$	SBcd	7.9	749	$4.8' \times 0.9'$	79°	12.04
ESO 209–9	FGCE 0684	$07^{\rm h}58^{\rm m}15.6^{\rm s}$	$-49°51'22''$	SBc	14.9	1119	$6.2' \times 0.9'$	82°	12.68
UGC 4559	FGC 103A	$08^{\rm h}44^{\rm m}08.0^{\rm s}$	$+30°07'07''$	Sb	27.8	2085	$3.2' \times 0.5'$	81°	14.10
NGC 2654	PGC 024784	$08^{\rm h}49^{\rm m}12.5^{\rm s}$	$+60°13'13''$	SBab	17.9	1342	$4.2' \times 0.8'$	79°	12.77
NGC 2683	UGC 04641	$08^{\rm h}52^{\rm m}41.0^{\rm s}$	$+33°25'03''$	Sb	5.5	410	$8.8' \times 2.6'$	77°	10.36
NGC 3003	UGC 5251	$09^{\rm h}48^{\rm m}36.0^{\rm s}$	$+33°25'18''$	SBc	19.7	1481	$6.0' \times 1.4'$	77°	12.15
NGC 3221	UGC 5601	$10^{\rm h}32^{\rm m}20.4^{\rm s}$	$+21°34'09''$	SBcd	54.8	4110	$3.2' \times 0.7'$	77°	13.80
NGC 3365	UGC 5878	$10^{\rm h}46^{\rm m}13.1^{\rm s}$	$+01°48'46''$	Sc	13.2	986	$4.4' \times 0.7'$	81°	13.04
NGC 3501	UGC 6116	$11^{\rm h}02^{\rm m}46.9^{\rm s}$	$+17°59'33''$	Sc	15.1	1133	$3.5' \times 0.5'$	82°	13.57
NGC 3600	UGC 6283	$11^{\rm h}15^{\rm m}52.1^{\rm s}$	$+41°35'27''$	Sab	9.6	1443	$4.1' \times 0.9'$	85°	12.60
NGC 3628	UGC 6350	$11^{\rm h}20^{\rm m}16.3^{\rm s}$	$+13°35'22''$	Sb	7.7	847	$14.8' \times 3.0'$	88°	10.42
NGC 3877	UGC 6745	$11^{\rm h}46^{\rm m}08.0^{\rm s}$	$+47°29'39''$	Sc	12.1	904	$5.3' \times 1.2'$	83°	11.85
NGC 3936	ESO 504–20	$11^{\rm h}52^{\rm m}20.4^{\rm s}$	$-26°54'24''$	SBbc	29.0	2022	$3.9' \times 0.6'$	81°	12.76
ESO 379–6	FGCE 0915	$11^{\rm h}53^{\rm m}03.1^{\rm s}$	$-36°38'20''$	Sbc	39.8	2986	$2.6' \times 0.4'$	81°	14.13
NGC 4206	IC 3064	$12^{\rm h}15^{\rm m}16.6^{\rm s}$	$+13°01'30''$	Sc	9.4	702	$5.2' \times 1.0'$	79°	12.80
NGC 4216	UGC 7284	$12^{\rm h}15^{\rm m}53.1^{\rm s}$	$+13°08'58''$	SBab	16.8	132	$7.9' \times 1.7'$	78°	10.95
NGC 4235	IC 3098	$12^{\rm h}17^{\rm m}08.9^{\rm s}$	$+07°11'31''$	Sa	32.1	2410	$3.8' \times 0.8'$	78°	12.64
NGC 4256	UGC 7351	$12^{\rm h}18^{\rm m}44.2^{\rm s}$	$+65°53'58''$	Sb	33.7	2528	$4.1' \times 0.7'$	80°	12.79
NGC 4388	UGC 7520	$12^{\rm h}25^{\rm m}47.0^{\rm s}$	$+12°39'42''$	Sb	33.6	2518	$5.5' \times 1.5'$	79°	11.91
NGC 4700	PGC 43330	$12^{\rm h}49^{\rm m}07.8^{\rm s}$	$-11°24'38''$	SBc	24.0	1407	$3.0' \times 0.6'$	78°	12.71
NGC 4945	ESO 219–24	$13^{\rm h}05^{\rm m}26.2^{\rm s}$	$-49°28'15''$	SBc	7.5	561	$20.4' \times 4.1'$	78°	9.15
NGC 5290	UGC 8700	$13^{\rm h}45^{\rm m}19.2^{\rm s}$	$+41°42'55''$	Sbc	34.4	2580	$3.7' \times 1.0'$	79°	12.93
NGC 5297	UGC 8709	$13^{\rm h}46^{\rm m}24.2^{\rm s}$	$+43°52'25''$	SBbc	67.5	2402	$5.4' \times 1.2'$	77°	12.37
NGC 5775	UGC 9579	$14^{\rm h}53^{\rm m}57.7^{\rm s}$	$+03°32'40''$	SBc	26.7	1681	$4.2' \times 1.0'$	82°	12.45
ESO 274–1	FGCE 1205	$15^{\rm h}14^{\rm m}13.6^{\rm s}$	$-46°48'45''$	Sd	7.0	522	$11.0' \times 1.6'$	82°	12.00
NGC 5965	UGC 9914	$15^{\rm h}34^{\rm m}02.1^{\rm s}$	$+56°41'10''$	Sb	45.5	3412	$4.7' \times 0.7'$	81°	13.21
NGC 6722	ESO 104–33	$19^{\rm h}03^{\rm m}39.6^{\rm s}$	$-64°53'41''$	Sab	76.7	5749	$2.9' \times 0.4'$	82°	13.56
IC 4837A	ESO 184–47	$19^{\rm h}15^{\rm m}15.7^{\rm s}$	$-54°07'57''$	Sab	38.0	2847	$4.1' \times 0.7'$	80°	12.55
ESO 142–19	PGC 63351	$19^{\rm h}33^{\rm m}18.0^{\rm s}$	$-58°06'50''$	S0-a	56.2	4211	$4.4' \times 1.1'$	81°	13.56

between UGC 260 and CGCG 434–012, which is barely visible in our R–band image. We cannot rule out in this particular case, that the eDIG emission is triggered by interaction of one of the nearby galaxies.

MCG-2-3-16

This edge–on galaxy is paired with another edge–on spiral, MCG-2-3-15. However, these two galaxies are not physically associated, as MCG-2-3-15 has a much higher radial velocity of $v_{\rm rad} = 5765\,{\rm km\,s^{-1}}$. Hence its H$\alpha$ emission is shifted outside the passband of the used Hα filter. MCG-2-3-16 on the other side is not very prominent in Hα. It is one of our 12 survey galaxies, which has no detectable FIR flux at 60μm or 100μm at the sensitivity of IRAS. A small arc is seen in the western portion, extending about 430 pc north of the disk, which is not extraplanar. The disk shows a slight asymmetry in thickness from east to

Table 2. continued

Galaxy[a]	alt. name	R.A. (J2000)	Dec. (J2000)	Type	D [Mpc]	$v_{\rm H\,I}$ [km s^{-1}]	$a \times b$	i	$m_{\rm B}$[b]
IC 4872	ESO 142–24	$19^{\rm h}35^{\rm m}42.3^{\rm s}$	$-57°31'10''$	SBc	25.7	1928	$3.5' \times 0.4'$	83°	14.03
NGC 6875A	ESO 284–24	$20^{\rm h}11^{\rm m}55.6^{\rm s}$	$-46°08'37''$	SBc	42.4	3176	$2.8' \times 0.5'$	80°	13.96
MCG-1-53-12	FGC 2290	$20^{\rm h}49^{\rm m}52.5^{\rm s}$	$-07°01'21''$	Sc	79.5	5965	$3.0' \times 0.4'$	82°	- - - -
IC 5052	ESO 74–15	$20^{\rm h}52^{\rm m}06.3^{\rm s}$	$-69°12'13''$	SBcd	7.9	591	$5.9' \times 0.9'$	81°	11.91
IC 5071	ESO 47–19	$21^{\rm h}01^{\rm m}19.7^{\rm s}$	$-72°38'33''$	SABb	41.6	3122	$3.4' \times 0.8'$	76°	13.28
IC 5096	ESO 107–19	$21^{\rm h}18^{\rm m}21.0^{\rm s}$	$-63°45'41''$	Sbc	41.9	3144	$3.1' \times 0.5'$	81°	13.30
NGC 7064	ESO 188–9	$21^{\rm h}29^{\rm m}02.4^{\rm s}$	$-52°45'58''$	SBc	11.4	858	$3.4' \times 0.6'$	80°	12.87
NGC 7090	ESO 188–12	$21^{\rm h}36^{\rm m}28.6^{\rm s}$	$-54°33'27''$	SBc	11.4	857	$7.7' \times 1.4'$	80°	11.47
UGC 11841	FGC 2351	$21^{\rm h}52^{\rm m}48.0^{\rm s}$	$+38°56'00''$	Scd	79.9	5990	$2.8' \times 0.2'$	86°	- - - -
NGC 7184	ESO 601–9	$22^{\rm h}02^{\rm m}38.5^{\rm s}$	$-20°48'47''$	SBc	34.1	2617	$6.0' \times 1.5'$	76°	11.91
IC 5171	ESO 288–46	$22^{\rm h}10^{\rm m}56.2^{\rm s}$	$-46°04'54''$	SBb	34.1	2850	$3.0' \times 0.4'$	82°	13.45
IC 5176	ESO 108–20	$22^{\rm h}14^{\rm m}54.5^{\rm s}$	$-66°50'46''$	SBbc	23.3	1746	$4.5' \times 0.5'$	84°	13.52
NGC 7339	UGC 12122	$22^{\rm h}37^{\rm m}46.9^{\rm s}$	$+23°47'14''$	SBbc	17.9	1343	$2.7' \times 0.7'$	80°	13.07
NGC 7361	IC 5237	$22^{\rm h}42^{\rm m}18.0^{\rm s}$	$-30°03'29''$	Sc	15.9	1245	$3.8' \times 1.0'$	80°	12.90
NGC 7412A	ESO 290–28	$22^{\rm h}57^{\rm m}07.0^{\rm s}$	$-42°48'15''$	SBd	12.4	929	$3.9' \times 0.6'$	81°	14.30
UGC 12281	FGC 2441	$22^{\rm h}59^{\rm m}12.4^{\rm s}$	$+13°36'21''$	Sc	34.2	2565	$3.5' \times 0.3'$	85°	14.79
NGC 7462	ESO 346–28	$23^{\rm h}02^{\rm m}46.5^{\rm s}$	$-40°50'02''$	SBbc	14.1	1061	$4.0' \times 0.9'$	84°	12.36
UGC 12423	FGC 2469	$23^{\rm h}13^{\rm m}06.0^{\rm s}$	$+06°24'00''$	Sc	64.5	4838	$3.4' \times 0.4'$	83°	14.41
NGC 7640	UGC 12554	$23^{\rm h}22^{\rm m}06.7^{\rm s}$	$+40°50'43''$	SBc	8.6	385	$9.9' \times 2.2'$	77°	11.46
ESO 240–11	FGCE 1839	$23^{\rm h}37^{\rm m}49.4^{\rm s}$	$-47°43'35''$	Sb	37.9	2843	$5.2' \times 0.5'$	84°	13.05

[a] All data have been taken from the RC3 (de Vaucouleurs et al. 1991), or have been calculated from those data, except where indicated

[b] taken from NED, and from (Schroeder & Visvanathan 1996)

west which might be a projection effect due to a slight deviation from the edge–on character.

UGC 1281

UGC 1281 was included in the Effelsberg/VLA radio continuum survey by Hummel et al. (1991). However, no radio halo was detected. The Hα image did not reveal any extraplanar DIG emission. UGC 1281 has also not been detected by IRAS, so this altogether hints for a low star formation activity. However, the Hα images show several bright H II regions in the disk which are not aligned. Two bright emission knots are slightly offset from the plane to the south.

UGC 2082

UGC 2082 is a northern edge–on spiral galaxy, which is located in the direction of the NGC 1023 group (Tully 1980). It has been investigated on the basis of a HST survey of large and bright nearby galaxies, studied with the FOC in the UV–regime at $\lambda \sim 2300$ Å (Maoz et al. 1996). However, UGC 2082 has not been detected, which is an indication that the SF activity within this galaxy is very low. That is reflected in our Hα images as well. We do not detect significant emission except some H II regions in the disk. The diagnostic FIR ratios are very low, too.

ESO 362–11

ESO 362–11 has a $\rm L_{FIR}/D_{25}^2$ ratio of ~ 2.6, which indicates a moderate SF activity. In our Hα images a weak layer of eDIG is found, but no filaments or plumes are detected. ESO 362–11 is listed in the catalog of Southern Peculiar Galaxies and Associations (Arp & Madore 1987) as AM 0514–370, possibly due to a chain of 4 galaxies which are located in the vicinity of ESO 362–11. These are on the outskirts of our covered field, and therefore are not shown in our appendix image. Telesco et al. (1988) report that galaxy interactions enhance the efficiency of SF activity, which is very likely. However, in the case of ESO 362–11 it is not clear, whether or not the chain of galaxies, which are not in the close vicinity of ESO 362–11, are able to enhance the SF activity. Coziol et al. (1998) even have classified ESO 362–11 on the basis of their *Pico Dos Dias Survey* as a starburst galaxy, based on FIR spectral indices.

ESO 209–9

This little studied nearby, southern edge–on galaxy has both a moderate ratio of $\rm L_{FIR}/D_{25}^2$, and S_{60}/S_{100}. Its Hα morphology reveals an extended layer, not as prominent as in NGC 891 or NGC 3044, but still quite intense. The distribution of the Hα emission is asymmetric which could be a projection effect, if we were looking at the very end of the spiral arm to the south along the line of sight, whereas the spiral arm to the north could be winded more tightly. Quite extraordinary is an additional emission component, which shows up in the whole field

Table 3. Journal of observations

Galaxy	Date	Telescope	Instrument	Hα filter Id.	$t_{\rm exp}$ (Hα) [s]	$t_{\rm exp}$ (R) [s]	Seeing [$''$]
NGC 24	01/08/2000	DAN1.54	DFOSC	ESO#693	2×2700	2×600	1.6
NGC 100	10/08/1999	CAHA2.2	CAFOS	CA#658/10	2×2700	$120 + 300$	
UGC 260	12/08/1999	CAHA2.2	CAFOS	CA#658/10	2×2700	$120 + 300$	1.5
ESO 540–16	01/08/2000	DAN1.54	DFOSC	ESO#693	2×2700	2×600	1.7
MCG-2-3-16	10/11/1999	DAN1.54	DFOSC	ESO#693	2×2700	$300 + 600$	1.2
NGC 360	10/07/1999	DAN1.54	DFOSC	ESO#697	2×2700	600	
NGC 669	13/08/1999	CAHA2.2	CAFOS	CA#665/17	2×2700	$120 + 300$	1.7
UGC 1281	12/08/1999	CAHA2.2	CAFOS	CA#658/10	2×2700	$120 + 300$	1.4
NGC 891	11/08/1999	CAHA2.2	CAFOS	CA#658/10	2×1800	$120 + 300$	2.0
UGC 2082	13/08/1999	CAHA2.2	CAFOS	CA#658/10	1×1800	300	
IC 1862	11/11/1999	DAN1.54	DFOSC	ESO#701	2×2700	$120 + 600$	1.5
NGC 1247	10/11/1999	DAN1.54	DFOSC	ESO#697	2×2700	$120 + 600$	1.6
ESO 117–19	22/02/1993	ESO2.2	EFOSC2	ESO#439	1×1800	900	
	22/02/1993	ESO2.2	EFOSC2	ESO#439	1×900	–	
IC 2058	10/11/1999	DAN1.54	DFOSC	ESO#693	1×2700	$120 + 600$	1.4
	10/11/1999	DAN1.54	DFOSC	ESO#693	1×2200	–	
ESO 362–11	11/11/1999	DAN1.54	DFOSC	ESO#693	2×2700	$120 + 600$	1.2
ESO 121–6	13/11/1999	DAN1.54	DFOSC	ESO#693	2×2700	$120 + 300$	1.3
NGC 2188	23/02/1993	ESO2.2	EFOSC2	ESO#694	2×1800	600	
ESO 209–9	13/11/1999	DAN1.54	DFOSC	ESO#693	2×2700	$120 + 300$	1.5
UGC 4559	22/02/1999	CAHA2.2	CAFOS	CA#658/10	2×1800	720	2.2
NGC 2654	21/02/1999	CAHA2.2	CAFOS	CA#658/10	2×1800	600	
NGC 2683	19/02/1999	CAHA2.2	CAFOS	CA#658/10	2×1800	600	1.4
NGC 3003	19/02/1999	CAHA2.2	CAFOS	CA#658/10	1×1800	800	1.5
	19/02/1999	CAHA2.2	CAFOS	CA#658/10	2×900	–	
NGC 3221	22/02/1993	ESO2.2	EFOSC2	ESO#439	1×1200	600	
	22/02/1993	ESO2.2	EFOSC2	ESO#439	1×900	–	
NGC 3365	21/02/1999	CAHA2.2	CAFOS	CA#658/10	2×1800	720	
NGC 3501	22/02/1999	CAHA2.2	CAFOS	CA#658/10	2×1800	720	
NGC 3600	20/02/1999	CAHA2.2	CAFOS	CA#658/10	2×1800	720	
NGC 3628	08/05/1991	NTT	EMMI	ESO#596	1×1800	300	
NGC 3877	20/02/1999	CAHA2.2	CAFOS	CA#658/10	2×1800	600	
NGC 3936	10/02/1995	NTT	EMMI	ESO#597	1×1200	300	
ESO 379–6	09/07/1999	DAN1.54	DFOSC	ESO#697	1×3600	2×600	1.4
NGC 4206	22/02/1999	CAHA2.2	CAFOS	CA#665/17	2×1800	720	3.0
NGC 4216	19/02/1999	CAHA2.2	CAFOS	CA#665/17	2×1800	600	
NGC 4235	20/02/1999	CAHA2.2	CAFOS	CA#665/17	2×1800	800	1.3
NGC 4256	21/02/1999	CAHA2.2	CAFOS	CA#665/17	2×1800	720	
NGC 4388	20/02/1999	CAHA2.2	CAFOS	CA#665/17	2×1200	500	
NGC 4700	01/08/2000	DAN1.54	DFOSC	ESO#693	2×2700	2×600	1.3
NGC 4945	09/07/1999	DAN1.54	DFOSC	ESO#693	1×2700	600	1.6
NGC 5290	21/02/1999	CAHA2.2	CAFOS	CA#665/17	2×1800	720	
NGC 5297	22/02/1999	CAHA2.2	CAFOS	CA#658/10	1×1800	720	2.0
	22/02/1999	CAHA2.2	CAFOS	CA#658/10	1×1300	–	
NGC 5775	07/05/1991	NTT	EMMI	ESO#595	1×1800	600	
ESO 274–1	01/08/2000	DAN1.54	DFOSC	ESO#693	2×2700	2×600	1.4
NGC 5965	09/08/1999	CAHA2.2	CAFOS	CA#665/17	2×2700	$120 + 300$	
NGC 6722	09/07/1999	DAN1.54	DFOSC	ESO#697	2×2700	600	
IC 4837A	08/07/1999	DAN1.54	DFOSC	ESO#697	2×2700	600	1.9
ESO 142–19	10/07/1999	DAN1.54	DFOSC	ESO#697	2×2700	600	1.8

around ESO 209–9. We speculate that this emission, which is shown in its fully covered extent in the Hα+continuum image (see Fig. 3), is of Galactic origin. Quite remarkably, there is no hint of any filamentary emission in the broad R–band image. Our first impression was that this could be straylight from a bright star just outside the covered CCD field. However, as there was neither a shift (after alignment) nor a change in the emission pattern noticed in the two individual Hα images, which were offset by $20''$ from one another, and furthermore such struc-

Table 3. continued

Galaxy	Date	Telescope	Instrument	Hα filter Id.	$t_{\rm exp}$ (Hα) [s]	$t_{\rm exp}$ (R) [s]	Seeing [″]
IC 4872	09/07/1999	DAN1.54	DFOSC	ESO#693	2×2700	600	1.7
NGC 6875A	10/07/1999	DAN1.54	DFOSC	ESO#697	2×2700	600	1.4
MCG-01-53-012	10/08/1999	CAHA2.2	CAFOS	CA#665/17	2×2700	$120 + 300$	1.3
IC 5052	08/07/1999	DAN1.54	DFOSC	ESO#693	2×2700	600	1.8
IC 5071	31/07/2000	DAN1.54	DFOSC	ESO#697	2×2700	2×600	1.9
IC 5096	12/11/1999	DAN1.54	DFOSC	ESO#697	2×2700	$120 + 300$	1.2
NGC 7064	12/11/1999	DAN1.54	DFOSC	ESO#693	2×2700	$120 + 600$	1.5
NGC 7090	09/07/1999	DAN1.54	DFOSC	ESO#693	1×1800	600	1.7
UGC 11841	11/08/1999	CAHA2.2	CAFOS	CA#665/17	2×2700	$120 + 600$	
NGC 7184	30/07/2000	DAN1.54	DFOSC	ESO#697	2×2700	$450 + 600$	1.5
IC 5171	31/07/2000	DAN1.54	DFOSC	ESO#697	2×2700	2×600	1.9
IC 5176	10/07/1999	DAN1.54	DFOSC	ESO#693	2×2700	600	1.8
NGC 7339	08/08/1999	CAHA2.2	CAFOS	CA#658/10	2×2700	$120 + 300$	1.7
NGC 7361	31/07/2000	DAN1.54	DFOSC	ESO#693	2×2700	600	1.7
NGC 7412A	13/11/1999	DAN1.54	DFOSC	ESO#693	2×2700	$120 + 600$	1.2
UGC 12281	10/08/1999	CAHA2.2	CAFOS	CA#665/17	2×2700	$120 + 300$	1.3
NGC 7462	11/11/1999	DAN1.54	DFOSC	ESO#693	2×2700	$120 + 600$	1.8
UGC 12423	09/08/1999	CAHA2.2	CAFOS	CA#665/17	1×2700	120	
NGC 7640	10/08/1999	CAHA2.2	CAFOS	CA#658/10	2×2700	$120 + 300$	
ESO 240–11	30/07/2000	DAN1.54	DFOSC	ESO#697	2×2700	2×600	2.0

tures were never recorded prior or after these exposures in other object frames, we suspect that these structures indeed have a Galactic origin. A visual inspection of both the blue and red DSS images did not reveal anything conclusive. Unfortunately, the IR DSS plate of the region around ESO 209–9 is not yet obtained/digitized. The IRAS maps show some emission in that area, however, the resolution is not sufficient enough to resolve these structures clearly. A possible explanation could be, that this emission is Galactic cirrus. This would not be unreasonable, since ESO 209–9 has a galactic latitude of only $b \approx -11°$. Unfortunately, this position is just outside the regions studied by the AAO/UKST Hα survey[4] of the southern galactic plane (e.g., Parker et al. 1999), which would have been a good test for comparison. It could also be extended red emission (ERE) in the diffuse interstellar medium. This ERE was found for high–galactic cirrus clouds by Szomoru & Guhathakurta (1998). They found a peak of cirrus ERE at λ ∼6000 Å. However, in order to unravel the true nature of this filamentary emission, this should be re–investigated by independent deep Hα images using a different instrumental setup, and supplemental spectroscopy. Fortunately, very recently, we downloaded an available Hα image from the Southern Hα Sky Survey Atlas (SHASSA)[5] (see Fig. 2), which became available very recently. For details on SHASSA we refer to Gaustad et al. (2001). Indeed, the field around the galaxy ESO 209–9 shows detectable Hα emission, and the Hα morphology is clearly recovered, despite the spatial resolution of the SHASSA is much lower than in our images.

[4] http://www.roe.ac.uk/wfau/halpha/halpha.html
[5] http://amundsen.swarthmore.edu/SHASSA/

Fig. 2. Field No. 51 of the Southern Hα Sky Survey Atlas (SHASSA), which includes the Galactic region in the direction of ESO 209–9. The field measures 13□°. The field around ESO 209–9 is indicated by a circle.

Fig. 3. Field around ESO 209–9, showing very structured, cirrus–like galactic emission in this Hα image. The corresponding R–band image does not show anything filamentary in the field of view. North is to the top and East is to the left. The field of view measures ∼ 13□′. Orientation: N is to the top and E to the left.

NGC 3003

NGC 3003 has been investigated spectroscopically by (Ho et al. 1995) in search of *dwarf* Seyfert nuclei, who concluded, based on a detected broad emission complex centered at λ4650Å, that this galaxy is a Wolf–Rayet galaxy. NGC 3003 has a modest $L_{\rm FIR}/D_{25}^2$ ratio (1.65), however, the S_{60}/S_{100} ratio of ∼0.34 hints that there is some SF activity due to enhanced dust temperatures. Furthermore, due to the slight deviation from its edge–on character, no extraplanar emission can be identified reliably. The Hα distribution, however, reveals strong planar DIG, consistent with the observations by Hoopes et al. (1999). Several bright emission knots can be discerned. About four decades ago a SN has been detected 34″E, and 17″N of the nucleus (SN 1961 F).

NGC 3221

This is one of the galaxies with the highest L_{FIR}/D_{25}^2 ratio in our survey (13.8). The S_{60}/S_{100} ratio is also quite high (0.37), suggesting enhanced SF activity. Indeed, there are many bright H II regions visible in the disk, preferentially located in the spiral arms, which are slightly recognizable, due to the small deviation from its edge–on inclination. A faint eDIG layer is visible. There is a slight asymmetry between the northern part and the southern part of the galaxy (i.e. the two spiral arms) discernable. NGC 3221 has also been investigated in the radio regime (radio continuum), where Irwin et al. (2000) detected extended disk emission. It is noteworthy to mention that a SN has been detected (SN 1961 L) in NGC 3221.

NGC 3501

NGC 3501 was observed with the Effelsberg 100m radio dish at 5 GHz in a survey to detect radio halos in edge–on galaxies, related to SF driven outflows (Hummel et al. 1991). No extended radio emission has been detected. The optical appearance, based on our Hα imaging reveals also a quiescent galaxy, with no extraplanar emission. Besides some modest H II regions in the disk, its morphology looks rather inconspicuous. In fact, it is also one of the 12 galaxies in our survey which has no FIR detections.

Fig. 4. Extraplanar DIG layer in NGC 3600. The eDIG morphology is reminiscent of a starburst galaxy. The field of view measures ∼11.3 kpc×11.3 kpc. Orientation: N is to the top and E to the left.

NGC 3600

This edge–on spiral galaxy has been included in the catalog of Markarian galaxies as Mrk 1443 (Mazarella & Balzano 1986). The broadband R image shows a prominent bulge and indicates a slight warp which was also noticed by (Sánchez–Saavedra et al. 1990). In our Hα image it becomes even more obvious that the disk is warped. There is some extraplanar DIG detected, basically around the central regions, where extended emission seems to be ejected from the nuclear region. There is, besides the nucleus, one bright emission region, presumably consisting of several smaller components, and several fainter knots visible in the disk. Although the L_{FIR}/D_{25}^2 is quite moderate (1.4), NGC 3600 has a relatively high S_{60}/S_{100} ratio of $\sim$ 0.44. Spectroscopy of the nuclear region reveals strong emission from the Balmer lines (Hα, Hβ), as well as from several forbidden low ionization lines, such as [N II], and [S II] (Ho et al. 1995). We show a detailed view of NGC 3600 in Fig. 4.

NGC 3628

NGC 3628 is a member of the *Leo triplet*, which also includes NGC 3623 and NGC 3627. It is a starburst galaxy with a very prominent dust lane, which obscures most parts of the emission in the galactic midplane. It has been studied extensively in almost all wavelength regimes, and has also been the target for a multi–wavelength study in the context of the disk–halo connection. Radio continuum observations (Schlickeiser et al. 1984) reveal extended emission, and in the X–ray regime a T$\sim 2\times10^6$ K, extended halo has been detected by sensitive PSPC observations with ROSAT (Dahlem et al. 1996). Prominent X–ray emission, tracing the collimated outflow from the nuclear starburst, was found to be spatially correlated with the Hα plume (Fabbiano et al. 1990). Extraplanar dust has already been detected (Howk & Savage 1999; Rossa 2001). We also observed extended emission from the nuclear outflow, localized extended emission (filamentary), and several extraplanar H II regions.

Fig. 5. Extraplanar DIG layer in NGC 3877 seen in this continuum subtracted Hα image. There is a pervasive eDIG layer clearly visible. The field of view measures 12 kpc×12 kpc. Orientation: N is to the top and E to the left.

Fig. 6. SN 1998 S (marked by a circle) in NGC 3877. Our R–band image was obtained 354 days after the discovery of SN 1998 S. Image size and orientation is same as above.

NGC 3877

NGC 3877 is a northern edge–on spiral galaxy, which ranks among the top 15 galaxies of our survey, according to the SFR per unit area. A SFR from observations in the UV has been derived, which yielded $0.55\,M_\odot\,yr^{-1}$ (Donas et al. 1987). A nuclear spectrum reveals quite strong emission of Hβ (Ho et al. 1995), whereas Hα, and the [N II] lines are also clearly detected. Just recently a SN of type II has been detected in NGC 3877, namely SN 1998 S (Filippenko & Moran 1998). In Fig. 6 we show our broadband R image, which was obtained almost a year after its discovery. The SN (marked by a circle), although considerably fainter, is still visible in our image. Niklas et al. (1995) report a λ2.8 cm flux for NGC 3877 of $S_{tot} = 23\pm8$ mJy. However, no radio map was shown, and they did not comment further on this galaxy. The Hα morphology, as seen in our images, reveal extended emission with some small filaments and plumes. Quite remarkable is the distribution of very strong H II regions and knots which are seen all over the disk (cf. Fig. 5). The nuclear region is very compact in Hα.

NGC 4216

Another Virgo cluster spiral, NGC 4216 has been classified as a WR–galaxy, based on detected He II λ4686 emission from a few regions within NGC 4216 (Schaerer et al. 1999). Pogge (1989b) investigated the morphology of

the nuclear emission, and concluded it as diffuse, while the circumnuclear region was characterized as faint and patchy. There is nuclear emission detected from X–rays (Fabbiano et al. 1992). Maoz et al. (1996) did not detect UV emission in NGC 4216 in their HST survey. Our Hα image did not reveal extraplanar emission. The nucleus is the strongest source, whereas several smaller H II regions in the outer spiral arm contribute also to the Hα emission.

NGC 4235

NGC 4235 has been classified as a Seyfert galaxy of type 1 (Weedman 1978), and has no physical companion (Dahari 1984). Pogge (1989a) has studied the nuclear environment using narrowband imaging of Hα and [O III]. He found a bright nucleus with an extended region towards the NE direction at P.A. $\sim 48°$, which extends $\sim 4.4''$. Neither disk H II regions were detected, nor ionized gas above the plane. Radio continuum observations (Hummel et al. 1991) also did not find evidence for extended emission. In the X–ray regime the strong nuclear region is detected with a luminosity of $1.55 \times 10^{42}\,\mathrm{erg\,s^{-1}}$ (Fabbiano et al. 1992). In a study of large–scale outflows in edge–on Seyfert galaxies Colbert et al. (1996b) found no double peaked line profiles, or any evidence for extended line regions, and no minor axis emission, too. However, on radio continuum images obtained with the VLA at 4.9 GHz there was a diffuse, bubble–like, extended structure (~ 9 kpc) found in addition to the unresolved nucleus (Colbert et al. 1996a). Our Hα image reveals a bright nucleus with a faint extended layer, which is restricted to the circumnuclear part. NE of the nucleus a depression is visible, possibly due to absorbing dust, as already noted by Pogge (1989a), and easily visible in the broad band HST image by Malkan et al. (1998). This is one of the very few Seyfert galaxies that appear in our survey. The role of minor axis outflows in Seyfert galaxies, and thus the contribution to the IGM enrichment and heating still has to be explored.

NGC 4388

NGC 4388 has been identified as the first Seyfert 2 galaxy in the Virgo cluster (Phillips & Malin 1982), and has been studied extensively in various wavelength regimes, including optical line imaging and spectroscopy (e.g., Keel 1983; Pogge 1988; Corbin et al. 1988), radio continuum (e.g., Stone et al. 1988; Hummel & Saikia 1991), and in the high energy waveband extended soft X–ray emission out to a radius of 4.5 kpc has been reported (Matt et al. 1994). From the optical morphology and kinematics it was derived that NGC 4388 possesses complex gas kinematics and is composed of several nucleated emission line regions. A prominent feature reaches out to $\sim 18''$ at P.A. $\sim 10°$ (Heckman et al. 1983). The radio continuum maps revealed a double peaked radio source close to the optical nucleus plus a cloud of radio emitting material, apparently ejected from the nucleus (e.g., Stone et al. 1988; Irwin et al. 2000).

Fig. 7. Continuum subtracted Hα image of NGC 4388, revealing an eDIG layer and an extended plume. The displayed area equals $\sim$36 kpc$\times$32 kpc at the distance of NGC 4388. Orientation: N is to the top and E to the left.

Some speculation on the true membership to the Virgo cluster exists, although NGC 4388 is located near the core of the Virgo cluster. This is because of its relatively high systemic velocity. However, most authors assume it is a member of the Virgo cluster. Therefore, ram pressure stripping seems to play a role as NGC 4388 interacts with the ambient intracluster medium (ICM). Optical narrowband imaging in Hα and [O III] has revealed that the morphology of the extended ionized gas is composed of two opposed radiation cones (Pogge 1988), which give rise to a *hidden Seyfert 1* nucleus, as favored in the *unification scheme* of AGN. Recent investigations of NGC 4388 using Fabry–Perot imaging techniques have revealed a complex of highly ionized gas $\sim$ 4 kpc above the disk (Veilleux et al. 1999). They found blueshifted velocities of $50 - 250\,\mathrm{km\,s^{-1}}$ NE of the nucleus. Furthermore they assume the velocity of the extraplanar gas to be unaffected by the inferred supersonic motion of NGC 4388 through the ICM of the Virgo cluster, and suggest that the galaxy and high–$|z|$ gas lies behind the Mach cone.

Our narrowband imaging of NGC 4388 (see Fig. 7) reveals also extended emission which is pointing away from the galactic disk to the halo in the NE direction. Furthermore a faint eDIG layer is visible. Very recently deep Hα images obtained with the Subaru telescope revealed very extended emission–line region in Hα and [O III] at distances of up to $\sim$35 kpc (Yoshida et al. 2002).

NGC 4700

NGC 4700 has been listed as a H II region galaxy in the list of Rodriguez Espinosa et al. (1987), while Hewitt & Burbidge (1991) list it as a Seyfert 2 galaxy. It has been included in the HST imaging survey of nearby AGN (Malkan et al. 1998). NGC 4700 has a relatively large ratio of S_{60}/S_{100} of $\sim$ 0.51, making it a promising candidate with a potential DIG halo according to the diagnostic DIG diagram. Indeed, a relatively bright, and extended gaseous halo with a maximum extent of 2.0 kpc above/below the galactic plane is discovered. One of the filaments can even be traced farther out to $\sim$ 3 kpc. The morphology of DIG in NGC 4700 is asymmetrical, with the eastern and middle part being most prominent. Five distinct bright H II region complexes, which are composed of several individual smaller regions across the disk, can be discerned. Some prominent filaments above active regions protrude from the disk into the halo. A small number of bright H II regions is seen in this part of the disk, and the maximum extent of the eDIG is visible above those regions. The western part of the galaxy is lacking in bright H II regions, hence the suppressed extend of the halo in this

Fig. 8. A detailed Hα view of NGC 4700 showing a bright and extended gaseous halo, superposed by individual filaments.

Fig. 9. The extended radio halo of NGC 4700 at ν=1.4 GHz (depicted in contours), overlaid onto the DSS image (Dahlem et al. 2001), courtesy M. Dahlem.

Fig. 10. A zoom onto the outflowing cone in this Hα image of NGC 4945. The displayed portion of this galaxy measures ∼5.6 kpc×5.6 kpc. Orientation: N is to the top and E to the left.

western part. NGC 4700 also bears an extended radio halo (radio thick disk), with the maximum extent correspondingly on the same position above the disk (Dahlem et al. 2001), although slightly more extended in the radio continuum image as in our Hα image (see Figs. 8+9).

NGC 4945

NGC 4945 is a well studied southern edge–on spiral galaxy, which belongs to the *Centaurus group*. It has been studied at various wavelengths, including the visual, IR, and radio regime. Heckman et al. (1990) found evidence for a starburst driven superwind in NGC 4945, and Moorwood & Olivia (1994) derive a ∼ 400 pc size starburst in addition to the presence of a visually absorbed Seyfert nucleus. They conclude that NGC 4945 is in an advanced stage of evolution from a starburst to a Seyfert galaxy. Extended emission from the disk was detected by radio continuum observations (Harnett et al. 1989; Colbert et al. 1996a), reaching a diameter of ∼ 23 kpc. X–ray emission was detected from the nuclear region, however, no extended emission was found in ROSAT PSPC observations (Colbert et al. 1998), probably due to quite large absorbing columns ($N_H = 1.5 \times 10^{21}$ cm^{-2}), as NGC 4945 is situated near the galactic plane ($b \sim 13°$). This decreases the sensitivity for the soft X–ray regime.

NGC 4945 is one of the few starburst galaxies that we have included in our Hα survey, and it is no surprise that it has the second highest L_{FIR}/D_{25}^2 ratio of ∼ 14.8 of our studied galaxies. Already investigated by Lehnert & Heckman (1995), NGC 4945 shows strong extraplanar DIG with many filaments protruding from the disk into the halo. There are at least two bright filaments on either side of the disk visible on our narrowband images. Several prominent dust patches, which obscure some parts of the emission south of the galactic plane is a further characteristic pattern for this galaxy. In Fig. 10 we show an enlargement of the middle part, which nicely shows the outflow cone from the nuclear starburst.

NGC 5290

Fig. 11. Continuum subtracted Hα image of NGC 5290, showing a pervasive eDIG layer and its morphology resembles those of a nuclear starburst galaxy. The displayed area measures ∼28.6,kpc×28.6 kpc at the distance of NGC 5290. Orientation: N is to the top and E to the left.

This northern edge–on galaxy is part of the LGG 361 group (Garcia 1993), which teams up with NGC 5289, which is located ∼ 13′ to the south, and has a velocity difference to NGC 5290 of ∼ 67 km s^{-1} (Huchra et al. 1983). In the optical NGC 5290's most striking character is a box–shaped bulge (de Souza & Dos Anjos 1987). The L_{FIR}/D_{25}^2 ratio is moderate (∼ 2.6), and NGC 5290 shows some extended emission, where a faint layer is detected, and some filaments, basically coming from the nuclear region and reaching into the halo, can be discerned (see Fig. 11). The morphology that is visible on the Hα image resembles those of a starburst galaxy, although NGC 5290 has no starburst–like FIR parameters, as the S_{60}/S_{100} ratio is considerably lower (0.31).

NGC 5297

Another northern edge–on spiral, NGC 5297 forms a binary galaxy with NGC 5296 (Turner 1976), which is separated by about 1.5′ from NGC 5297, and has a velocity difference of $\Delta v \approx 360$km s^{-1}. Another interesting source is also located in the direct vicinity, a quasar of V=19.3 mag (Arp 1976). This quasar ([HB89] 1342+440), which has a redshift of $z = 0.963$, is located 2.5′ to the SW. Arp reports on a luminous extension from NGC 5236 pointing at the QSO, which Sharp (1990) did not confirm. However, Sharp (1990) did comment on the unusually bright off–center secondary nucleus of NGC 5296. The QSO is marked by a circle in our R–band image in Fig. 40. The outer spiral arms of NGC 5297 show evidence of perturbation by the S0 companion, as reported by (Rampazzo et al. 1995).

Radio continuum observations of NGC 5297 have been performed (Hummel et al. 1985; Irwin et al. 1999, 2000). While Irwin et al. (1999) claims extended radio continuum emission from NGC 5297, still, higher resolution observations show only very weak emission (Irwin et al. 2000). Our Hα image does not reveal any extraplanar emission. Thus, we do not see enhanced SF activity due to the interaction with the companion galaxy in this case. The L_{FIR}/D_{25}^2 ratio is moderate. We also note, that this galaxy actually is not perfectly edge–on.

NGC 5775

From H I observations it was found that NGC 5775 is an interacting galaxy with its neighbor face–on spiral NGC 5774. Emission along a bridge has been detected, although no tidal arms are discovered (Irwin

1994). NGC 5775 is a good studied northern edge–on galaxy in the disk–halo context, which has been imaged in Hα (Lehnert & Heckman 1995; Collins et al. 2000; Tüllmann et al. 2000), where extraplanar emission was detected out to over 5 kpc above the galactic plane. It is the galaxy with the highest L_{FIR}/D_{25}^2 ratio in our sample and is a starburst–type galaxy, although no clear indications exist on a nuclear starburst. A bright halo with individual filaments superposed in a prominent *X–shape* are discovered on our narrowband image, consistent with earlier observations, mentioned above. Extraplanar DIG has been detected spectroscopically out to 9 kpc (Rand 2000; Tüllmann et al. 2000), and extended radio continuum emission has been detected as well (Hummel et al. 1991; Duric et al. 1998). Extended X–ray emission coexistent with a radio continuum spur and optical filament was discovered on ROSAT PSPC archival images (Rossa 2001).

ESO 274–1

ESO 274–1 belongs to the *Cen A* group of galaxies, and Banks et al. (1999) derive a H I mass of $430 \times 10^6\,M_\odot$, ranking on position five of the *Cen A* group. This little studied southern edge–on galaxy was included in the recent list of dwarf galaxies by Cote et al. (1997), who studied new discovered dwarf galaxies in the nearest groups of galaxies. From optical inspection of the DSS images, it is obvious that this galaxy has a low surface brightness. It is the galaxy with the lowest L_{FIR}/D_{25}^2 ratio among the IRAS detected galaxies in our sample (0.19)! Quite remarkably however, the S_{60}/S_{100} ratio is among the highest in our sample, making ESO 274–1 a promising candidate in search for eDIG. We show in Fig. 12 an enlargement of the most active SF regions, which show strong local extended emission. The SW and middle part is most prominent, whereas there are regions in the NE part, where this galaxy (superposed by a crowded field of foreground stars) is almost invisible in Hα.

ESO 142–19

This is a perfect edge–on galaxy, and it is the only one of type S0–a in our sample. It was only included because of its classification as type Sa in the NED. It shows a strong dust lane, and a strikingly bright, and extended bulge in the R–band image. An upper radio continuum flux limit of 20 mJy at λ11 cm has been given by Sadler (1984), and a upper flux limit of $F_{[N\,II]} < 1.6 \times 10^{-14}\,erg\,s^{-1}\,cm^{-2}$ has been derived by Phillips et al. (1986). We detect no extended emission in ESO 142–19. Even the disk is almost invisible on our Hα image.

IC 5052

IC 5052 is a late–type spiral with classifications Scd or Sd. Radio emission detected by λ35 cm observations revealed an unusually double peaked radio emission complex associated with the disk, which was not coming from the nucleus (Harnett & Reynolds 1991).

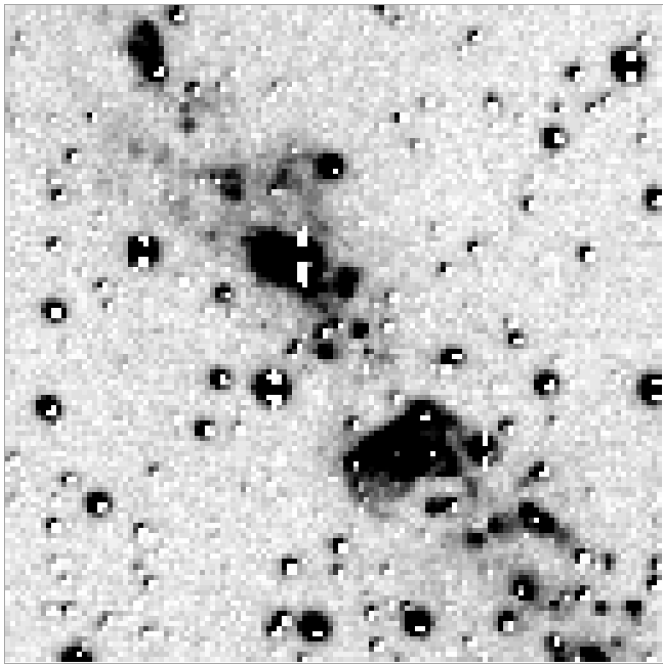

Fig. 12. Prominent extraplanar emission regions in this continuum subtracted Hα image of ESO 274–1. The displayed area equals $\sim$4.4 kpc$\times$4.4 kpc at the distance of ESO 274–1. Orientation: N is to the top and E to the left.

Our Hα image reveals a bright layer of extraplanar DIG superposed by individual filaments and shells (see Fig. 13). There is a depression in the Hα distribution noticed in the southern part of the galaxy, due to significant dust absorption, which almost separates the galaxy in two parts. An asymmetrical distribution is also visible in the R–band image. The southern edge is dominated by Hα emission, whereas the broadband image shows almost no intensity. Several arcs and shells make this galaxy a good target for further high resolution studies.

Paα observations with NICMOS 2 HST (Böker et al. 1999) showed excess emission of an isolated region in the disk–halo interface, slightly offset from the disk, which is possibly associated with one of the brighter emission regions in the southern part of our Hα image. The diagnostic ratios are both moderate, so it is quite remarkable that extended DIG emission is detected in that abundance in IC 5052.

NGC 7064

NGC 7064 is a H II region like galaxy (Kirhakos & Steiner 1990). Radio emission has been detected at λ35 cm (Harnett & Reynolds 1991), which extends over the inner disk with a maximum intensity at the nucleus. The disk emission is more pronounced to the east, which corresponds to the optical emission distribution. They further show in their map a weak extension to the south, which apparently has no optical counterpart. NGC 7064 has also been detected in the ROSAT All Sky Survey (RASS), which was included in a study of IRAS galax-

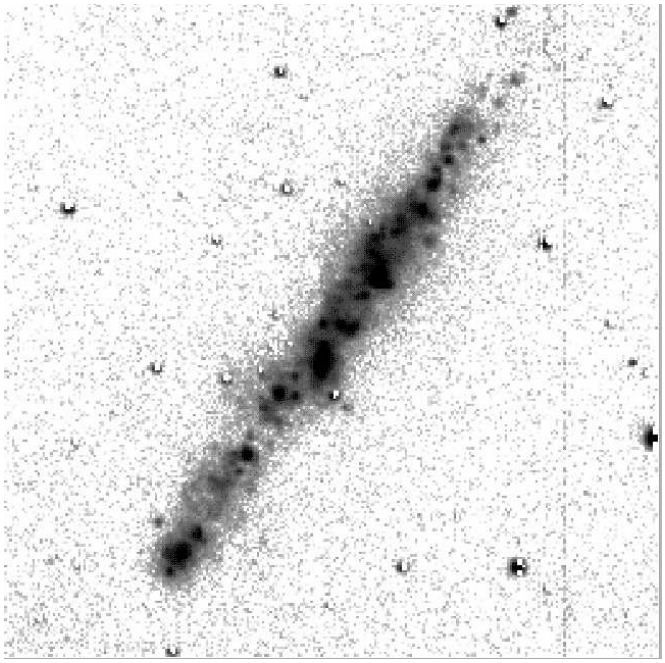

Fig. 13. Continuum subtracted Hα image of IC 5052, showing an eDIG layer, filaments and shells. The displayed area is ∼11.8 kpc×11.8 kpc. Orientation: N is to the top and E to the left.

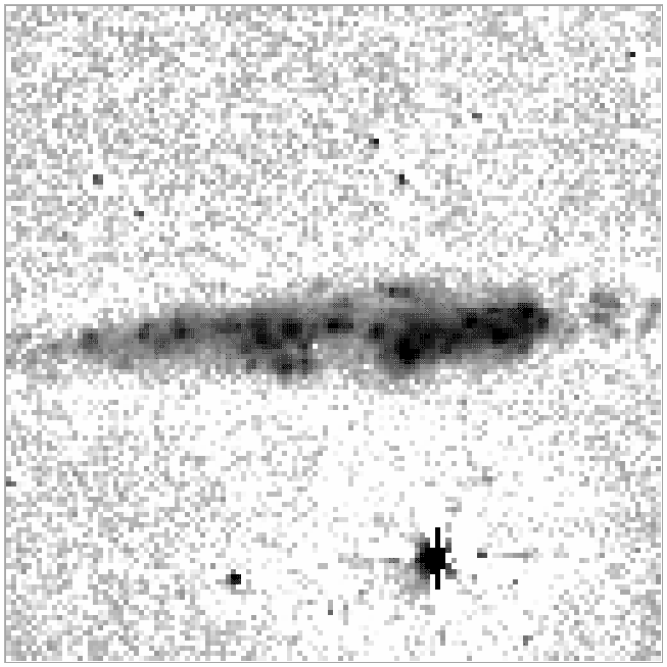

Fig. 14. Continuum subtracted Hα image of NGC 7064, revealing a faint extraplanar DIG layer. The displayed area measures ∼10.0 kpc×10.0 kpc. Orientation: N is to the top and E to the left.

ies (Boller et al. 1998). The X–ray intensity maximum is offset from the IRAS position (nucleus). Furthermore, weaker emission is detected to the south of NGC 7064 at larger distances far out in the halo region. Presently it is not clear if it is related to NGC 7064. In Fig. 14 we show our Hα image, scaled logarithmically, to show the faint halo. A few emission patches and plumes are visible to the south of the disk, and also in the northern part. The disk emission is asymmetrically distributed, with the eastern part being most prominent. There is a prominent hole in the southern disk, bisecting the disk almost entirely. In our logarithmically scaled image the hole is almost filled with diffuse emission, but its intensity is weaker than in the eastern and western part of the disk–halo interface. Although the L_{FIR}/D_{25}^2 ratio is quite low, it should be noted that the S_{60}/S_{100} ratio is the highest in our sample.

NGC 7090

This southern edge–on spiral has radio continuum detections at λ 35 cm (Harnett & Reynolds 1985). The radio emission follows the plane of the galaxy, and extends above it in two distinct spurs out to a distance of ∼ 1.5 kpc. The radio peak coincide with the optical nucleus, however, they note no obvious nuclear radio source. Our R–band image shows that a prominent dust lane with patchy structures runs across most parts of the disk offset slightly to the north. It is very irregular, unlike most other prominent dust lanes, such as in NGC 891 or IC 2531. The Hα image (Fig. 15) reveals a faint halo, in addition to some filaments and extended emission in the form of knots. The northeastern part of the galaxy has the highest intensity in emission, whereas the southern half is almost absent, except very few emission patches (H II regions) in the disk. The filaments protrude basically from the nuclear region into the halo. It should be noted that the extended radio continuum emission is coincident with the Hα extended emission.

NGC 7184

NGC 7184 was detected in the radio regime at λ20 cm continuum emission (Condon 1987), and bears a double peaked brightness distribution. This was confirmed by Harnett & Reynolds (1991), who detected two maxima at λ35 cm. NGC 7184 is located at a projected distance of 163 kpc (20.9′) to NGC 7185, as quoted by Kollatschny & Fricke (1989), who studied the group environment of Seyfert galaxies. A peculiar supernova was detected in NGC 7184, named SN 1984 N (Barbon et al. 1999). Our Hα image did not show any extraplanar emission, which might be due to the fact, that NGC 7184 is not perfectly edge–on. The outstanding feature in NGC 7184 is the inner ring, which is also prominently seen on the R–band image. There is a well pronounced sub–structure visible, and several H II regions can be discerned in the ring and in the outer spiral arms.

NGC 7339

The late type spiral NGC 7339 is accompanied by the galaxy NGC 7332 at a projected distance of 5.2′, the latter

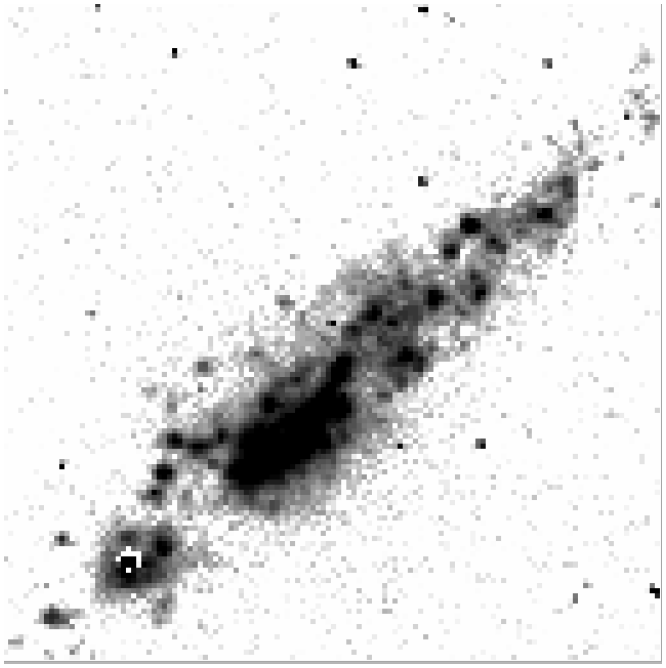

Fig. 15. Continuum subtracted Hα image of NGC 7090, showing an eDIG layer, with filaments and plumes. The displayed area of the galaxy measures ∼7.8 kpc×7.8 kpc. Orientation: N is to the top and E to the left.

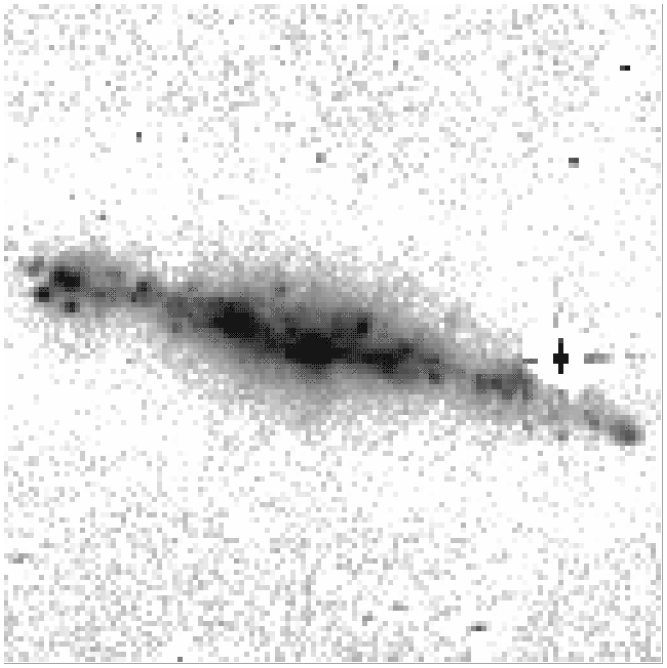

Fig. 16. Continuum subtracted Hα image of NGC 7462, showing extraplanar emission. The displayed area equals ∼10 kpc×10 kpc at the distance of NGC 7462. Orientation: N is to the top and E to the left.

one being a peculiar S0 galaxy, which has a velocity difference of $\Delta v = -141\,\mathrm{km\,s^{-1}}$ in comparison to NGC 7339. A supernova (SN 1989 L) has been discovered in NGC 7339 (Barbon et al. 1999). Several bright, and compact knots are seen in our Hα image, but no extraplanar emission is detected. NGC 7332, which is also visible on our frame, is completely absent in Hα.

UGC 12281

UGC 12281 has already been studied in the DIG context a few years ago by Pildis et al. (1994). They claim to have detected two extraplanar emission line features (discrete clouds), and a clumpy plume. We can confirm the presence of these two clouds, and the plume is also marginally detected in our image, which suffers from low S/N.

NGC 7462

This southern edge–on spiral was detected with the VLA at ν=1.49 GHz (Condon et al. 1987), and Maoz et al. (1996) have conducted UV observations at (λ2300 Å) of the inner $22'' \times 22''$ region with the HST, where they detected a *star-forming* morphology in several distinct regions (knots). Our Hα image (Fig. 16) reveals an extended DIG layer with individual plumes and faint filaments superposed. The disk emission is composed of several distinct emission complexes, clustered basically in three regions (nucleus + two regions within the disk), and some fainter regions in the outskirts of the disk.

UGC 12423

UGC 12423 belongs to the Pegasus I cluster of galaxies, and was once reported being one of the most massive and luminous spirals, with a derived H I mass of $\sim 9 \times 10^9\,\mathrm{M_\odot}$, and $\log \mathrm{M_H/L_B} = +0.14$ (Bothun et al. 1982; Schommer & Bothun 1983). Hummel et al. (1991) did not detect extended emission from UGC 12423 in their radio continuum survey. Our Hα image also does not show any extraplanar emission. The galaxy is almost invisible in Hα. This can partly be attributed to insufficient S/N, as we unfortunately only acquired one exposure for Hα, and also the R–band image was not long enough integrated. This needs to be re–investigated with more sensitive observations.

3.3. Hα sensitivities and error budgets of the continuum subtraction

From the direct comparison of the distribution of eDIG in the galaxies in our survey, with those already observed by Lehnert & Heckman (1995) and Rand (1996), we can conclude that we have reached similar and in a few cases somewhat better sensitivities. This is mostly true for the galaxies, which were obtained with DFOSC at La Silla. The Calar Alto observations, however, have been acquired through relatively wide Hα filters in several cases ($\Delta\lambda \sim 168$ Å), so the sensitivity is not as good as for the La Silla observations, which were made through Hα filters of $\Delta\lambda \sim 62$ Å. The estimated mean sensitivities of the galaxies observed with DFOSC are of the order of a few $\mathrm{cm^{-6}\,pc}$.

Typically there are some uncertainties associated with the scaling procedure, to be applied for the continuum subtraction. The scaling factor has been determined from the ratio of the Hα and continuum countrates of individual stars in the object frames. Of course, there arise uncertainties as the actual continuum spectrum of a galaxy will be different from that of individual stars, as the galactic continuum is the superposition of all stars of the underlying stellar population. However, practice has shown, that this is a good method and the uncertainties typically are of the order of 5–10 %. A careful analysis, however, is necessary in order to match the ideal scaling factor. The determined factor from the intensity ratio of the stars in the Hα and continuum frame has been slightly changed in a few cases where the derived scaling factor did not seem to match perfectly, as artifacts were observed in the bulge region, which is a good indicator for the accuracy of the scaling process. Then the galaxy profile was analyzed carefully, as the scaling factor was changed in very small steps to find the optimal (in a somewhat conservative manner) value, not to under- and oversubtract the emission. This is a well established procedure (for more details see e.g., Hoopes et al. 1999; Rossa & Dettmar 2000).

Alternatively, it is possible to determine the scaling factor using continuum regions in the galaxy. This is something which would work much better for *face–on* galaxies, but is somewhat more difficult for *edge–on galaxies*, as here occasionally the prominent dust lane makes it difficult to assess whether there is underlying emission, which is strong enough to be seen after subtracting the continuum. Furthermore, the true Hα emission is only revealed after the continuum subtraction process. Hence, knowing regions free of emission is somewhat difficult to judge, prior to the subtraction process. However, testing this method, applied to a few individual galaxies, have shown that there is a good agreement between using stars or continuum light within the galaxies for the determination of the scaling factor.

3.4. Discussion

This first large Hα survey of edge–on galaxies has shown that eDIG is a general phenomenon *only* for galaxies which exceed a minimal threshold of SF activity. As already suggested by Rand (1996) and Rossa & Dettmar (2000), the results presented in this work corroborate this view that a considerable fraction of late–type spirals indeed show extended DIG emission in their galactic halos. Although not as common as in starburst galaxies eDIG is a widespread phenomenon and is not a characteristic belonging only to a small fraction of late–type spirals. For details concerning the interpretation of our data we refer to Rossa & Dettmar (2003, Paper I).

Evidence for the disk–halo interaction has also been gathered from observations tracing other constituents of the ISM, such as the hot ionized medium (HIM) (Bregman & Pildis 1994; Dahlem 1997), and dust (Howk & Savage 1999). The latter constituent is also briefly discussed for our survey galaxies in the following section.

4. Extraplanar dust

As a by–product of our continuum subtraction process the R–band images were also used to study another important constituent of the ISM, namely the dust. Edge–on galaxies are ideally suited candidates for this kind of investigation, since the dust lane is clearly visible in projection, although it should be noted that not all edge–on galaxies bear a bright and filamentary dust lane. In recent studies of the edge–on spiral NGC 891, using high spatial resolution broad band imaging in various filterbands, high latitude dust features have been discovered (Howk & Savage 1997; Rossa 2001). Hundreds of dust features are recognized from which over a dozen individual dust features have already been studied in more detail (Howk & Savage 1997). They are located at distances of $300\,\mathrm{pc} \leq z \leq 1500\,\mathrm{pc}$ above the galactic plane. Although other investigations dealing with dust in edge–on galaxies have been carried out in the past (e.g., Sofue 1987; Sofue et al. 1994), the recent works by Howk & Savage (1997, 1999) are one of the first linking the extraplanar dust features to the interaction between the disk and the halo of the galaxy, although Sofue (1987) already argued that the dust features might be connected to a magnetic process termed *magnetic fountain*.

4.1. Analysis

In order to study the individual dust features in more detail the R–band images have been processed to enhance the visibility of the dust structures against the galaxy background. As performed in the studies by Howk & Savage (1997, 1999), we have similarly applied an unsharp–masking method to our R–band images. We have gaussian–filtered the images with a FWHM of 10–15 pixels for the different data sets. Then the original R–band frames have been divided by the gaussian-filtered images to produce the final unsharp–masked images. By applying this procedure to the whole frame, point sources with high count–rates (i.e. bright stars) appear as artifacts.

The detection of individual dust features is a straightforward method, since in the positive grey scale images the white structures (i.e. the dust) clearly separated from other morphological features which are recognizable in the galaxy background (stars, remaining cosmics, gas, background galaxies). This method was only applied to enhance the visibility. Possible artifacts, which arise due to the smoothing process, can easily be identified on the original R–band frames. However, the detection of extraplanar dust features rests on several galaxy parameters. The inclination is a very important factor. Galaxies with inclinations $i \leq 80°$ do not separate the prominent dust lane clearly enough in projection. The distribution of dust fil-

Fig. 17. Unsharp–masked R–band image of IC 2135, showing very patchy dust filaments. No continuous dust lane is visible. N is on top, and E is to the left.

Fig. 18. Unsharp–masked R–band image of NGC 4302, showing spectacular dust features above/below the galactic plane. The face–on spiral to the right is NGC 4298. N is on top, and E is to the left.

Fig. 19. Unsharp–masked R–band image of NGC 4402. Several dust filaments, which reach high galactic latitudes, are visible. N is on top, and E is to the left.

aments along the dust lane can be quite different for each galaxy, which is partly due to a projection effect, and partially attributed to the intrinsic morphology and distribution of the dust within each galaxy.

4.2. Results

The unsharp–masked greyscale images of the survey galaxies are shown in Figs. 17–20 (the galaxies from our first sub–sample Rossa & Dettmar 2000) and all others in Figs. 22–54 (only available electronically at EDP Sciences) in the central rows (between the R–band and Hα images) in order of their increasing R.A.. Each figure consists of 2×3 sub–panels, with two galaxies, each one accompanying one column. The scale is marked by a black horizontal bar in the lower corner of each figure, and the orientation is N to the top, and E to the left.

The following results are obtained from the simple analysis of the unsharp–masked R–band images. We find extraplanar dust (eDust) filaments in 26 of our 74 galaxies. 48 galaxies lack in showing extraplanar dust. In one case (ESO 274–1) we cannot state with confidence whether there are eDust filaments visible or not, as this galaxy is superimposed onto a crowded field of foreground stars. The unsharp–masked process caused many artifacts, therefore no clear statement can be given in this particular case. We count this galaxy as a negative detection in our statistics, which is summarized in Table 4. Typical distances of the extraplanar dusty filaments from the galactic midplane are $|z| \sim 0.6 - 1.5\,\mathrm{kpc}$.

The dust structures at high galactic latitudes are diverse in morphology. In IC 2135[6], where no prominent dust lane is detected, only patchy features are seen in the disk–halo interface on both sides of the disk (cf. Fig. 17). Very spectacular filamentary structures are discovered in NGC 4302 (Fig. 18). Many of the discovered dusty filaments are strongly bended, suggesting that magnetic fields may act upon the charged dust particles. The *Virgo Cluster* spiral NGC 4402 (see Fig. 19) shows strongly winded filaments, which are detectable out to $|z| \sim 1.7\,\mathrm{kpc}$. The dusty structures show a disturbed morphology as well as the eDIG morphology. This suggests that ram–pressure stripping, caused by the interaction of the ISM with the ambient *Virgo Cluster* Intracluster Medium (ICM), is acting upon NGC 4402. This has been concluded for other *Virgo Cluster* galaxies as well (e.g., Veilleux et al. 1999; Vollmer et al. 2000). In Fig. 20 we show the remaining six of the nine galaxies studied in Hα by Rossa & Dettmar (2000).

[6] IC 2135 was inadvertently identified with NGC 1963 in Rossa & Dettmar (2000), due to a general confusion in the literature and in electronic databases that existed back then.

Table 4. eDust detections / non–detections

eDust	no eDust	pos. corr.	neg. corr.
n=26	n=48	n=66	n=8
35%	65%	89%	11%

Candidate galaxies with prominent dusty features at high galactic latitudes include two starburst galaxies NGC 3628, NGC 5775, and also the galaxy NGC 7090. The unsharp–masked images can be seen in the Figs. 35, 41, 48, respectively.

The distribution of the high–$|z|$ dust features reveals that *usually extraplanar dust is visible in those galaxies, where also eDIG is detected*. The dust features, however, reach much lower galactic latitudes, except in two cases – NGC 360, NGC 4302 – where dust is detected at larger distances from the galactic midplane than eDIG. Generally, the distribution of the high–$|z|$ dust is restricted to $|z| \leq 1.5\,\mathrm{kpc}$.

We find two cases, where eDust was detected (NGC 360, ESO 240–11), but where no eDIG has been detected. On the other side, we find six cases where the opposite is true. The majority (89 %), however, shows a clear correlation between eDIG/eDust detections and non–detections. Although a correlation of the presence/non–presence of high–$|z|$ gas and dust exists, it should be noted that *in general* no 1:1 correlation exists (i.e. individual gas and dust filaments are not spatially correlated)! This might indicate that other mechanisms are responsible for the transport of the dust into the halo, than for the gas transport.

4.3. Discussion

The presented results of this investigation of the extraplanar dust distribution in edge–on galaxies are in very good agreement with those by Howk & Savage (1999, 2000). They investigated a small sample of 12 nearby edge–on spirals using multicolor broad band (B and V) observa-

tions (Howk & Savage 1999). Four of their studied objects are also covered in our Hα survey, namely NGC 891, NGC 3628, NGC 4302, and NGC 4634. Based on their small sample they derive physical properties for a few individual dust features. They derive large column densities of $3 \times 10^{20}\,\mathrm{cm}^{-3} \leq \mathrm{N_H} \leq 2 \times 10^{21}\,\mathrm{cm}^{-3}$, and derive dust masses of $\sim$ a few $10^5\,\mathrm{M}_\odot$. Although their observations have been carried out in the B, and V bands, and our observations were performed in the somewhat more transparent R–band, we find a good general agreement between their and our data for the structure of the high–$|z|$ dust features.

The coincidence of high latitude gas and dust structures suggests that these both phases of the ISM are most likely tied to the same driving force, the star formation processes in the underlying galaxy disk. However, the mechanism for the dust ejection might be different from the ones responsible for expelling the gas to high galactic latitudes. While models for the gas transport include magneto–hydrodynamic (MHD) flows such as the *galactic fountains* (Shapiro & Field 1976), *chimneys* (Norman & Ikeuchi 1989), favored expulsion models for the dust may be considered via radiation pressure on dust grains, termed *photolevitation* (e.g., Franco et al. 1991; Ferrara et al. 1991), and flows initiated by magnet field instabilities (*Parker instabilities*), caused by SNe explosions (e.g., Parker 1992; Shchekinov et al. 2001).

The reason to assume that the two distinct phases of the ISM are expelled by different processes is justified by the basic notion, that dust grains in the harsh environments of the star formation processes will be completely destroyed, and should not be observed at high galactic latitudes.

5. Summary and conclusions

The detection of star formation driven gaseous outflows using the Hα narrow band line imaging techniques is a viable method to trace the distribution of the warm ionized medium in external galaxies on a global scale. Many of the actively star-forming galaxies show similar, yet different, morphologies as the starburst galaxies.

We have presented the individual results for the Hα survey galaxies. From the 74 investigated edge–on spirals we have detected eDIG in 30 galaxies, that is 40.5%. We can therefore conclude, that *the presence of eDIG* in halos of galaxies is not a unique case for only a few galaxies, rather it *is found to be ubiquitous in galaxies, which exceed a certain level of SFR per unit area*, or even at a fainter threshold in combination with enhanced dust temperatures Rossa & Dettmar (2003). However, it can thus also be concluded that eDIG is not a common feature among *all* late–type spiral galaxies, as many of them do not show eDIG (at the level of the observed sensitivities). The presence of eDIG is depending on the SF activity on both local and global scales.

The morphology of eDIG shows a wide variety ranging from individual plumes, and filaments in galaxies with mediocre SF activity, to pervasive layers in the actively SF galaxies. A few of our eDIG detected targets bear a more or less intense layer of extended emission with typical extraplanar distances of 1.5–2 kpc. Individual filaments of some galaxies (e.g., NGC 4388, NGC 5775) even reach distances of up to $\sim$ 6 kpc. In the case of NGC 4700 a good correlation between extended Hα emission and radio continuum (radio halo) is found, which further strengthens the disk–halo interaction scenario.

Acknowledgements. It is our sincere pleasure to express our thanks to Dr. Francisco Prada for carrying out some of the observations at Calar Alto in an emergency case. We owe special thanks to Dr. Michael Dahlem for providing us with the data on NGC 3936, kindly observed by Dr. Eva Grebel. We would also like to thank the anonymous referee for his/her helpful comments. The authors would like to thank Deutsches Zentrum für Luft– und Raumfahrt (DLR) for financial support of this research project through grant 50 OR 9707. Additional travel support for the Calar Alto observing runs is acknowledged from the DFG through various grants. This research has made extensive use of the NASA/IPAC Extragalactic Database (NED) which is operated by the Jet Propulsion Laboratory, California Institute of Technology, under contract with the National Aeronautics and Space Administration. The Southern Hα Sky Survey Atlas (SHASSA) is supported by the National Science Foundation.

Fig. 20. Unsharp–masked R–band images. Upper left: NGC 3044, upper right: IC 2531, middle left: NGC 4634, middle right: NGC 5170, lower left: IC 4351, lower right: UGC 10288. The corresponding Hα images can be found in Rossa & Dettmar (2000). Orientation: N is to the top and E to the left.

Table 5. DIG morphology of the survey galaxies

Galaxy	DIG morph.[a]	vertical extent $\|z\|$ [kpc]	radial extent R_{SF} [kpc]	Notes
NGC 24	d, n	0.68	3.09	not perfectly inclined
NGC 100	n	0.63	5.82	H II regions in the disk
UGC 260	eh2, f, h_f, pec	2.00	7.14	pec = tidal debris?, galaxy?
ESO 540–16	d	0.73	7.88	strong asymmetry of planar DIG
MCG-2-3-16	a, n	0.43	2.67	disturbed disk
NGC 360	d	0.59	11.71	
NGC 669	n		28.33	
UGC 1281	n	0.42	3.34	H II regions not aligned
NGC 891	ee, eh2, f, h_b	2.15	9.85	eDIG asymmetry (north–south)
UGC 2082	d, n	0.44	4.68	
IC 1862	d, n		47.17	slightly warped disk
NGC 1247	d, pa		36.10	
ESO 117–19	d		27.89	
IC 2058	n	0.48	7.66	
ESO 362–11	h_f	2.47	7.80	
ESO 121–6	h_f	1.42	7.88	
NGC 2188	ee, eh2, f, pl	1.35	6.18	
ESO 209–9	h_b, pa, pl	1.57	12.60	+ galactic emission
UGC 4559	n	1.00	6.29	disk em. restr. near nucleus
NGC 2654	d, n	1.18	7.18	clustered H II regions
NGC 2683	d, n	0.87	2.63	strong disk emission
NGC 3003	d, n		9.35	galaxy not perfectly edge–on
NGC 3221	ee, h_f	3.82	35.27	
NGC 3365	d, n	1.00	2.23	strong local disk emission
NGC 3501	n	0.85	7.19	disk H II regions not aligned
NGC 3600	ee	1.24	4.20	nuclear outflow?, warped disk
NGC 3628	ee, eh2, f	3.13		prominent nuclear outflow
NGC 3877	ee, f, pl	1.38	12.00	clustered DIG emission
NGC 3936	n		11.46	
ESO 379–6	ee, pl	2.08	25.23	
NGC 4206	d, pa	1.22	8.02	
NGC 4216	d, n		11.48	strong Hα bulge emission
NGC 4235	ee, h_f	2.50	4.58	dust obscur. near nucleus
NGC 4256	d, n		13.17	planar DIG asymmetry
NGC 4388	f, h_f, pa	5.92	15.50	prominent halo patch
NGC 4700	h_b, f, pa	2.18	12.50	one filament $z \approx 3$ kpc
NGC 4945	f, h_b, pl	5.28	$\geq$22.42	outflow cone
NGC 5290	ee, f, h_b	4.00	13.00	nucl. outflow, starburst?
NGC 5297	d, n		16.00	not perfectly edge–on
NGC 5775	h_b, f, pl	5.38	21.44	prominent filaments
ESO 274–1	ee, f	0.75		strong local eDIG
NGC 5965	d, n		19.78	
NGC 6722	n		42.86	warped disk
IC 4837A	d		13.57	strong local DIG
ESO 142–19	n			prominent dust lane
IC 4872	n	0.71	3.33	
NGC 6875A	ee?, pa	2.75	12.00	not perfectly edge–on
MCG-01-53-012	n	1.40	10.80	
IC 5052	a, ee, h_b, pl	1.24	9.90	DIG distr. asymmetrically
IC 5071	d		20.85	clustered DIG emission
IC 5096	n	1.00	19.61	strong bulge emission
NGC 7064	ee, h_f, pl	0.92	7.20	disk bi–sected
NGC 7090	a, ee, f, h_f	1.78	8.39	strong local emission
UGC 11841	n			gal. barely vis. in Hα
NGC 7184	d, n		20.44	strong emission in annulus

Table 5. continued

Galaxy	DIG morph.[a]	vertical extent $\|z\|$ [kpc]	radial extent R_{SF} [kpc]	Notes
IC 5171	d		10.19	strong planar DIG
IC 5176	ee, h_f	2.35	10.22	
NGC 7339	n	0.36	2.32	disk H II regions not aligned
NGC 7361	d, n		9.49	strong disk emission
NGC 7412A	a, n	0.47	4.77	bright disk H II regions
UGC 12281	n	1.36	20.00	
NGC 7462	f, h_f, pl	1.76	10.81	slight asymmetry
UGC 12423	n			gal. barely vis. in Hα
NGC 7640	d, n		7.11	strong planar DIG
ESO 240–11	n		29.93	slight disk asymmetry

[a] a=arc(s), *d*=disk emission (only planar DIG), ee=extended emission (locally), eh2=extraplanar H II region(s), f=filament(s), h_b=bright halo, h_f=faint halo, n=no (e)DIG, pa=patch(es), pec=peculiar, pl=plume(s)

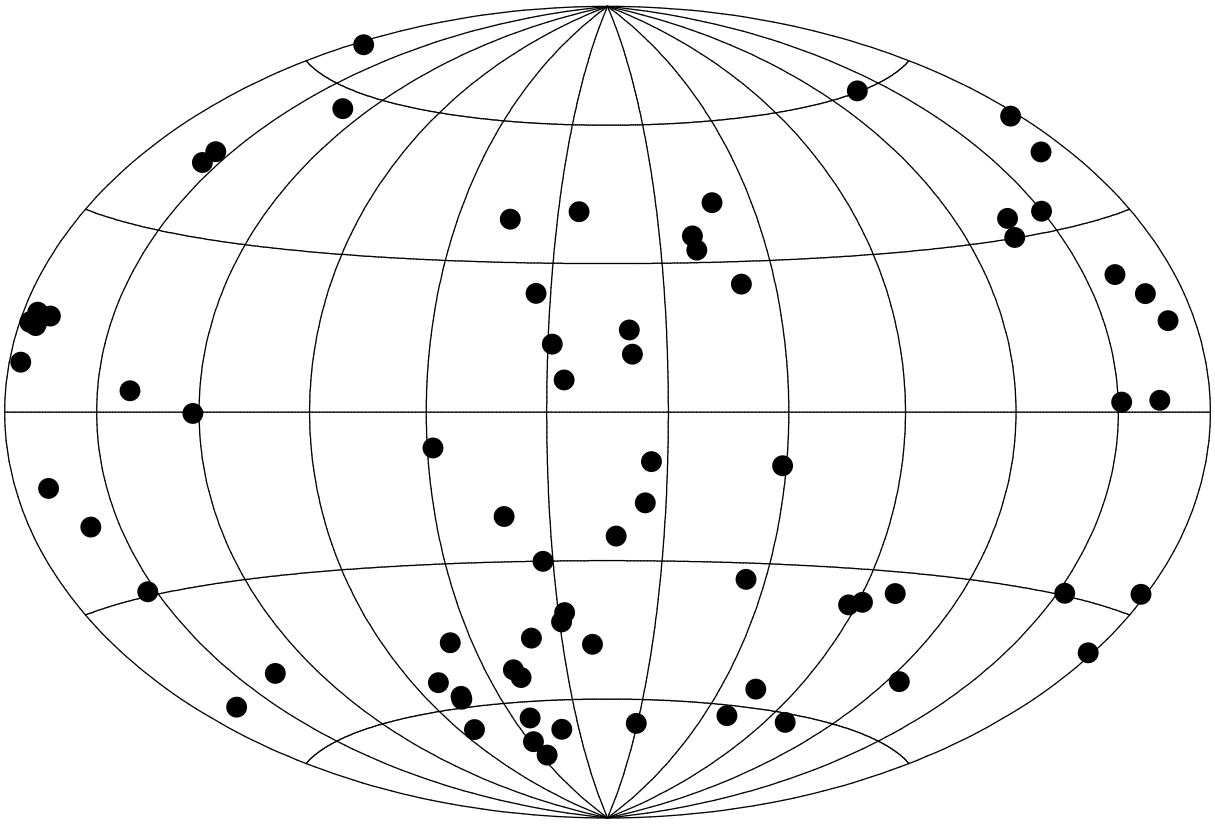

Fig. 21. Distribution of the observed 74 galaxies of the Hα survey on the celestial sphere in Aitoff projection. The center position is 0,0 in R.A., Dec.

References

Arp, H.C. 1976, ApJ, 210, L59

Arp, H.C., & Madore, B.F. 1987, Catalogue of Southern Peculiar Galaxies and Associations, Cambridge University Press

Banks, G.D., Disney, M.J., Knezek, P.M., et al. 1999, ApJ, 524, 612

Barbon, R., Buondi, V., Cappellaro, E., & Turatto, M. 1999, A&AS, 139, 531

Böker, T., Calzetti, D., Sparks, W., et al. 1999, ApJS, 124, 95

Boller, T., Bertoldi, F., Dennefeld, M., & Voges, W. 1998, A&AS, 129, 87

Bothun, G.D., Skillman, E., & Balick, B. 1982, AJ, 87, 1098

Bregman, J.N., & Pildis, R.A. 1994, ApJ, 420, 570

Colbert, E.J.M., Baum, S.A., Gallimore, J.F., O'Dea, C.P., & Christensen, J.A. 1996a, ApJ, 467, 551

Colbert, E.J.M., Baum, S.A., Gallimore, J.F., et al. 1996b, ApJS, 105, 75

Colbert, E.J.M., Baum, S.A., O'Dea, C.P., & Veilleux, S. 1998, ApJ, 496, 786

Collins, J.A., Rand, R.J., Duric, N., & Walterbos, R.A.M. 2000, ApJ, 536, 645

Condon, J.J. 1987, ApJS, 65, 485

Condon, J.J., Yin, Q.F., & Burstein, D. 1987, ApJS, 65, 543

Corbin, M.R., Baldwin, J.A., & Wilson, A.S., 1988, ApJ, 334, 584

Cote, S., Freeman, K.C., Carignan, C. & Quinn, P.J. 1997, AJ, 114, 1313

Coziol, R., Torres, C.A.O., Quast, G.R., Contini, T., & Davoust, E. 1998, ApJS, 119, 239

Dahari, O. 1984, AJ, 89, 966

Dahlem, M. 1997, PASP, 109, 1298

Dahlem, M., Heckman, T.M., Fabbiano, G., Lehnert, M.D., & Gilmore, D. 1996, ApJ, 461, 724

Dahlem, M., Lazendic, J.S., Haynes, R. F., Ehle, M., & Lisenfeld, U. 2001, A&A, 374, 42

de Souza, R.E., & Dos Anjos, S. 1987, A&AS, 70, 465

Dettmar, R.–J. 1990, A&A, 232, L15

Dettmar, R.–J. 1992, Fund. Cosm. Phys., 15, 148

de Vaucouleurs G., de Vaucouleurs A., Corwin H. G., et al. 1991, Third Reference Catalogue of Bright Galaxies (RC 3), Springer Verlag

Domgörgen, H., & Dettmar, R.–J. 1997, A&A, 322, 391

Donas, J., Deharveng, J.M., Laget, M., Milliard, B., & Huguenin, D. 1987, A&A, 180, 12

Duric, N., Irwin, J.A., & Bloemen, H. 1998, A&A, 331, 428

Fabbiano, G., Heckman, T.M., & Keel, W.C. 1990, ApJ, 355, 442

Fabbiano, G., Kim, D.–W., & Trinchieri, G. 1992, ApJS, 80, 531

Ferguson, A.M.N., Wyse, R.F.G., Gallagher, J.S., III, & Hunter, D.A. 1996, AJ, 112, 2567

Ferrara, A., Ferrini, F., Barsella, B., & Franco, J. 1991, ApJ, 381, 137

Filippenko, A.V., & Moran, E.C. 1998, IAUC 6830

Franco, J., Ferrini, F., Barsella, B., & Ferrara, A. 1991, ApJ, 366, 443

Garcia, A.M. 1993, A&AS, 100, 47

Gaustad, J.E., McCullough, P.R., Rosing, W., & Van Buren, D. 2001, PASP, 113, 1326

Guthrie, B.N.G. 1992, A&AS, 93, 255

Harnett, J.I., & Reynolds, J.E. 1985, MNRAS, 215, 247

Harnett, J.I., & Reynolds, J.E. 1991, A&AS, 88, 73

Harnett, J.I., Wielebinski, R., Haynes, R.F., & Klein, U. 1989, A&A 216, 39

Heckman, T.M., Armus, L., & Miley, G.K. 1990, ApJS, 74, 833

Heckman, T.M., van Breugel, W., Miley, G.K., & Butcher, H.R. 1983, ApJS, 88, 1077

Hewitt, A., & Burbidge, G. 1991, ApJS, 75, 297

Ho, L.C., Filippenko, A.V., & Sargent, W.L. 1995, ApJS, 98, 477

Hoopes, C.G., Walterbos, R.A.M., & Rand, R.J. 1999, ApJ, 522, 669

Howk, J.C., & Savage, B.D. 1997, AJ, 114, 2463

Howk, J.C., & Savage, B.D. 1999, AJ, 117, 2077

Howk, J.C., & Savage, B.D. 2000, AJ, 119, 644

Huchra, J., Davis, M., Latham, D., & Tonry, J. 1983, ApJS, 52, 89

Hummel, E., & Saikia, D.J. 1991, A&A, 249, 43

Hummel, E., Beck, R., & Dettmar, R.–J. 1991, A&AS, 87, 309

Hummel, E., Pedlar, A., Davies, R.D., & van der Hulst, J.M. 1985, A&AS, 60, 293

Irwin, J.A. 1994, ApJ, 429, 618

Irwin, J.A., English, J., & Sorathia, B. 1999, AJ, 117, 2102

Irwin, J.A., Saikia, D.J., & English, J. 2000, AJ, 119, 1592

Keel, W.C. 1983, ApJS, 52, 279

Kirhakos, S.D., & Steiner, J.E. 1990, AJ, 99, 1722

Kollatschny, W., & Fricke, K.J. 1989, A&AS, 219, 34

Lehnert, M.D., & Heckman, T.M. 1995, ApJS, 97, 89

Malkan, M.A., Gorjian, V., & Tam, R. 1998, ApJS, 117, 25

Maoz, D. Filippenko, A.V., Ho, L.C., et al. 1996, ApJS, 107, 215

Matt, G., Piro, L., Antonelli, L.A., et al. 1994, A&A, 292, L13

Mazzarella, J.M., & Balzano, V.A. 1986, ApJS, 62, 751

Moorwood, A.F.M., & Olivia, E. 1994, ApJ, 429, 602

Niklas, S., Klein, U., Braine, J., & Wielebinski, R. 1995, A&AS, 114, 21

Norman, C.A., & Ikeuchi, S. 1989, ApJ, 345, 372

Parker, E.N. 1992, ApJ, 401, 137

Parker, Q.A., Phillipps, S., & Morgan, D.H. 1999, in: "New Perspectives on the Interstellar Medium", ASP Conf. Series Vol. 168, eds. A.R. Taylor, T.L. Landecker, and G. Joncas, p. 126

Phillips, M., & Malin, D.F. 1982, MNRAS, 199, 905

Phillips, M.M., Jenkins, C.R., Dopita, M.A., Sadler, E.M., & Binette, L. 1986, AJ, 91, 1062

Pildis, R.A., Bregman, J.N., & Schombert, J.M. 1994, ApJ, 427, 160
Pogge, R.W. 1988, ApJ, 332, 702
Pogge, R.W. 1989a, ApJ, 345, 730
Pogge, R.W. 1989b, ApJS, 71, 433
Rampazzo, R., Reduzzi, L., Sulentic, J.W., & Madejsky, R. 1995, A&AS, 110, 131
Rand, R.J. 1996, ApJ, 462, 712
Rand, R.J. 2000, ApJ, 537, L13
Rand, R.J., Kulkarni, S.R., & Hester, J.J. 1990, ApJ, 352, L1
Rand, R.J., Kulkarni, S.R., & Hester, J.J. 1992, ApJ, 396, 97
Reshetnikov, V., & Combes, F. 1996, A&AS, 116, 417
Rodriguez Espinosa, J.M., Rudy, R.J., & Jones, B. 1987, ApJ, 312, 555
Rossa, J. 2001, Ph.D. thesis, Ruhr–University Bochum, Germany
Rossa, J., & Dettmar, R.–J. 2000, A&A, 359, 433
Rossa, J., & Dettmar, R.–J. 2003, A&A, in press (Paper I)
Sadler, E.M. 1984, AJ, 89, 53
Sánchez–Saavedra, M.L., Battaner, E., & Florido, E. 1990, MNRAS, 246, 458
Schaerer, D., Contini, T., & Pindao, M. 1999, A&AS, 136, 35
Schlickeiser, R., Werner, W., & Wielebinski, R. 1984, A&A, 140, 277
Schommer, R.A., & Bothun, G.D. 1983, AJ, 88, 577
Schroeder A., Visvanathan N. 1996, A&AS, 118, 441
Shapiro, P.R., & Field, G.B. 1976, ApJ, 205, 762
Sharp, N.A. 1990, PASP, 102, 109
Shchekinov, Yu.A., Dettmar, R.–J., Schröer, A., & Steinacker, A. 2001, in: "European Astronomy at the turn of the millennium": JENAM 2000, in press, (astro-ph/0102164)
Sofue, Y. 1987, PASJ, 39, 547
Sofue, Y., Wakamatsu, K.–I., & Malin, D.F. 1994, AJ, 108, 2102
Stone, J.L., Wilson, A.S., & Ward, M.J. 1988, ApJ, 330, 105
Szomoru, A., & Guhathakurta, P. 1998, ApJ, 494, L93
Telesco, C.M., Wolstencroft, R.D., & Done, C. 1988, ApJ, 329, 174
Tüllmann, R., Dettmar, R.–J., Soida, M., Urbanik, M., & Rossa, J. 2000, A&A, 364, L36
Tully, R.B. 1980, ApJ, 237, 390
Turner, E.L. 1976, ApJ, 208, 20
Veilleux, S., Bland–Hawthorn, J., Cecil, G., Tully, R.B., & Miller, S.T. 1999, ApJ, 520, 111
Vollmer, B., Marcelain, M., Amram, P., et al. 2000, A&A, 364, 532
Weedman, D.W. 1978, MNRAS, 184, P11
Yoshida, M., Yagi, M., Okamura, S., et al. 2002, ApJ, 567, 118